Identification of non-oncology drugs with activity against inflammatory and triple-negative breast cancer cell lines

SYED AHMAD, SARA KANDIL, KEVIN P. WILLIAMS and JOHN E. SCOTT

Department of Pharmaceutical Sciences, Biomanufacturing Research Institute and Technology Enterprise, North Carolina Central University, Durham, NC 27707, USA

Received July 22, 2025; Accepted November 7, 2025

DOI: 10.3892/ol.2025.15428

Abstract. Inflammatory breast cancer (IBC) and triple-negative breast cancer (TNBC) are subtypes of breast cancer with the lowest 5-year survival rates. One potential approach to increase survival rates for these cancers may be to identify tolerable and inexpensive daily maintenance therapies that could be administered in between standard of care treatments. The present study aimed to identify non-oncology drugs (NODs) that show activity against IBC/TNBC that could be repurposed for this use. Thus, a collection of NODs were screened and curated from a published database using cell line SUM-149, which is both an IBC and TNBC cell line (TN-IBC). In a parallel screening approach, a subset of these NODs were tested for activity against two other TNBC cell lines. Together, 15 drugs with activity against this IBC cell line were identified and grown as spheroids. A number of these drugs have not been previously identified as having activity in an IBC cell line. In addition, eight of these were understudied for TNBC and, therefore, they were tested against three TNBC cell lines grown as spheroids, resulting in variable breadth of activities. Drug potency (GI_{50}) was also assessed relative to their C_{max} reported in human studies. Eltrombopag, a thrombocytopenia drug, was active against SUM-149 and two other TNBC cell lines with a GI_{50}:C_{max} ratio of ~1. Papaverine, a vasodilator, was also active against SUM-149 and one other TNBC cell line with a GI_{50}:C_{max} ratio of ~2. Mozavaptan, a hyponatremia drug, inhibited proliferation in 4 out of 5 cell lines (all except SUM-149) with GI_{50}=2.7-7.6 μM (C_{max} unknown). Spironolactone (GI_{50}:C_{max}=10) had anti-proliferative activity only against SUM-149, suggesting a unique vulnerability. Overall, our data indicated that eltrombopag, papaverine and other identified NODs may have potential for being repurposed for TN-IBC and TNBC in general.

Introduction

In the clinic, breast cancer (BC) has been commonly characterized by the absence or presence of three key proteins: estrogen receptor (ER), progesterone receptor) and the growth factor receptor HER2 (1). This information allows clinicians to choose specific treatment options that target these receptors. BC that lacks the expression of all three of these proteins is termed triple-negative breast cancer (TNBC). In the case of TNBC, the drugs developed to target these proteins are ineffective and standard chemotherapy is employed to treat most patients. TNBC represents 15-20% of BC cases and it is the most aggressive subtype of breast cancer with the lowest 5-year survival rate (2). Gene expression profiling provides an additional method to subtype BC into five sub-groups according to their gene transcription patterns: Luminal A, Luminal B, HER2, basal and normal-like (3). The basal subtype has significant overlap with the TNBC subtype and its characteristics. TNBC will frequently respond to chemotherapy initially but subsequently grow back more aggressive and resistant to therapy. It is also more likely to metastasize than other subtypes. Due to this re-growth and metastasis after initial positive response to chemotherapy, there is a need for safe and tolerable daily maintenance therapy that can slow or prevent this re-growth.

Inflammatory breast cancer (IBC) is a rare type of BC accounting for 2-6% of all breast cancer cases, however, it accounts for 10% of all BC deaths (4,5). IBC is primarily characterized by its clinical presentation that includes diffuse skin thickening known as peasu d'orange phenomenon, edema, erythema, nipple abnormalities and swelling of the breast (6,7). These characteristics typically have a rapid onset within a six-month period, may or may not include a palpable lump and

Correspondence to: Dr John E. Scott, Department of Pharmaceutical Sciences, Biomanufacturing Research Institute and Technology Enterprise, North Carolina Central University, 1801 Fayetteville Street, BRITE Building, Durham, NC 27707, USA
E-mail: jscott@nccu.edu

Abbreviations: BC, breast cancer; TNBC, triple-negative breast cancer; IBC, inflammatory breast cancer; TN-IBC, triple-negative inflammatory breast cancer; DMSO, dimethyl sulfoxide; GI, growth inhibition; CTG, CellTiter Glo; FBS, fetal bovine serum; 2-D, two-dimension; NOD, non-oncology drug; C_{max}, maximal concentration; SD, standard deviation; ER, estrogen receptor; FDA, Food and Drug Administration; ATCC, American Type Tissue Collection; TPOR, thrombopoietin receptor; V2R, vasopressin V2 receptor; NER, nucleotide excision repair; AR, androgen receptor

Key words: inflammatory breast cancer, triple-negative breast cancer, eltrombopag, papaverine, mozavaptan, spironolactone

can be readily mistaken for infection or other breast conditions. These distinctive visible hallmarks of IBC are caused by tumor emboli blocking lymphatic ducts. IBC is an extremely aggressive type of BC that has frequently metastasized by the time of diagnosis. Although IBC clinically presents differently than other BC subtypes, it is still evaluated and categorized into the above subtypes (e.g., TNBC) and these biomarkers used to guide treatment options. Thus, a case of IBC may also be subtyped as triple-negative, referred to here as TN-IBC. TN-IBC has the lowest survival rate within the IBC classification, compared to ER+ and HER2+ subtypes (8). The standard of care for IBC is neoadjuvant chemotherapy (traditional or targeted, depending on subtype), radical mastectomy and then radiation post-mastectomy (4,9).

While progress has been made in identifying drugs for TNBC, e.g., PARP and immune checkpoint inhibitors, there is still a lack of therapies specifically targeting triple-negative forms of breast cancer. Drug repurposing is the identification of new clinical applications for existing, Food and Drug Administration (FDA)-approved drugs, thereby reducing the time and financial cost associated with the traditional drug discovery process (10). In addition, due to already known clinical and safety data reducing the need for extensive preclinical testing, the repurposed drug may be less expensive for the patient and healthcare system. In the cancer field, drug repurposing can entail either the repurposing of cancer drugs approved for a different type of cancer or the use of non-oncology drugs (NODs). NODs are FDA-approved (or other agencies) drugs that were originally approved for indications other than cancer. Many NODs have been discovered to have activity against specific cancers *in vitro* and *in vivo* (10). These NODs hold the potential to be less toxic than standard chemotherapy. These unique NODs may be administered simultaneously with chemotherapy to enhance efficacy or reduce the dose of the more toxic chemotherapies.

We propose additional use of NODs with anti-cancer activity. New therapies are needed to reduce the risk of relapses and slow cancer re-growth/metastasis in the interval after standard treatments have completed-thus providing constant therapy to the patient. We propose that tolerable, low toxicity NODs with anticancer activity may serve as maintenance therapy that could be taken on a regular basis for the interval between standard of care treatments or after they are completed. This maintenance therapy is envisioned to reduce the risk of recurrence or slow cancer re-growth and metastasis, attenuating disease progression in the interval between standard of care treatments. NODs are especially well suited for this purpose due to their much better safety and tolerability profiles that may allow daily dosing, unlike toxic chemotherapy agents.

In this report, we sought to identify NODs with activity against TN-IBC and TNBC. We employed the SUM-149 cell line grown in spheroid culture as a model assay for TN-IBC. We used this assay to screen a collection of NODs identified and curated from a published database based on the screen of drugs against standard TNBC cell lines (among others), but not IBC cell lines. In parallel, we also tested a subset of these NODs against other TNBC cell lines grown in two-dimension (2-D) culture. We identified 15 NODs with activity against SUM-149. Eight of these were also tested against a panel of TNBC cell lines grown in spheroid culture to assess breadth of activity. Several drugs, including eltrombopag and papaverine, may have potential for repurposing for these aggressive cancers.

Materials and methods

Materials. Plasticware and general reagents, including dimethyl sulfoxide (DMSO), were obtained from Fisher Scientific. Cell culture media and supplements were obtained from ThermoFisher and Hyclone (GE Healthcare). CellTox Green stock solution and the CellTiter Glo (CTG) 2.0 cell viability reagent were purchased from Promega. Paclitaxel and cycloheximide were purchased from Sigma-Aldrich; Merck KGaA. The drugs were purchased from SelleckChem with a stated purity of ≥97%. D300 Digital Dispenser and T4 and T8 cassettes were purchased from Tecan.

Cell culture. The cell lines MDA-MB-231, HCC-1806 and Hs578T were obtained from American Type Tissue Collection (ATCC). MDA-MB-231 and Hs578T were grown in DMEM supplemented with 10% fetal bovine serum (FBS) and Hs578T media was further supplemented with 0.01 mg/ml insulin. HCC-1806 were cultured in RPMI-1640 with 10% FBS. SUM-149 and SUM-159 were obtained from BioIVT. These cell lines were grown in DMEM/F12 supplemented with 10 mM HEPES, 5% FBS, 5 μg/ml insulin, 20 ng/ml EGF and 1 μg/ml hydrocortisone. The media for all the cell lines were further supplemented with 2.5 mM L-glutamine, 100 U/ml penicillin and 100 U/ml streptomycin. The cells were grown in tissue-culture treated flasks in a humidified incubator at 37˚C and 5% CO_2 and cells were harvested for assays with trypsin-EDTA (Versene). Cell lines were tested periodically for mycoplasma using the MycoAlert kit (Lonza, Basel, Switzerland) and they tested negative for mycoplasma. The cell lines were obtained directly from the vendors which authenticated the cell lines. ATCC uses STR profiling to authenticate their cell lines. All cell lines were amplified and stored frozen within 2-3 passages from original cells provided by the vendor. Experiments were performed with cells that were less than twenty passages from the vendor supplied cells.

Spheroid growth and cytotoxicity assays. For the initial single concentration screening of the 48 drugs with SUM-149, we used a combination of real time imaging using a real-time microscopic imaging instrument (Incucyte S3, Sartorius) to monitor spheroid area and fluorescence from the CellTox Green cytotoxicity dye and subsequently, CTG was employed to detect viable cells by ATP detection. The cell lines were harvested, counted with a Vi-Cell XR Cell Viability Analyzer (Beckman Coulter) and then plated in 96-well plates (Sbio, Catalog # MS-9096UZ) at 5,000 cells/well in 100 μl/well complete growth media. The plate was centrifuged at 200 x g for 10 min and then put in the incubator for 72 h for spheroid formation. Subsequently, the drugs and dye were added the same day. CellTox Green dye was added to all wells at 1:1,000 final dilution (100 nl) of the stock solution using the D300 Digital Dispenser with T8 cassettes. Immediately after dye addition, the D300 was used to directly deliver compounds dissolved in DMSO or DMSO only (for solvent control wells) to create single point tests or 8-point half-log serial dilutions (for follow up concentration response

assays). The D300 was employed to adjust DMSO in all wells to the same final DMSO concentration of 0.1% with T8 or T4 cassettes following the manufacturer's protocol for the instrument. Subsequently, the assay plates were put into the imaging instrument and monitored every 4 or 6 h. After 96 h, 50 or 100 μl of CTG was added to the wells, plate shaken 5 min and then incubated at room temp for 30 min covered by aluminum foil to protect from light before luminescence detected by Pherastar (BMG) or GloMax Explorer (Promega) plate readers. The Incucyte Spheroid (Sartorius) software module was used to determine spheroid area by phase contrast and total green fluorescence of the well. The initial measurement for spheroid area (0 h) was subtracted from the final measurement for each well (96 h) to determine change in area of the spheroid for each well. This change in area reflects spheroid growth during the assay, while the total fluorescence reflected a change in accessible DNA which reflects cytotoxicity. Time 0 fluorescence values were used to check for autofluorescence of the compound that may be the source of higher fluorescence. Change in area of each well (spheroid) was normalized to the mean of the change in area of the DMSO only wells (used as 100% growth) to obtain percent of control which reflected growth of spheroid. Total fluorescence was normalized to 'no cells' (media only) wells and DMSO wells. Thus, values >100% represented cytotoxicity. Similarly, luminescence from the CTG part of the assay was normalized using the mean of 'no cells' wells (0% viability) and DMSO control wells (100% viability). Known cytotoxic drug paclitaxel (0.1 μM) and cycloheximide (10 μM; primarily an inhibitor of cell proliferation) were used as controls to confirm detection of cell death and inhibition of cell proliferation, respectively. The CTG single concentration data was assessed for statistical significance using unpaired t-test to identify active hits, defined as significantly ($P<0.05$) less than 100% of control.

For subsequent assays to calculate the concentration of drug that produced 50% growth inhibition (GI_{50}), only the CTG assay was performed as above. To establish the signal representing no cell proliferation, a zero-day control plate was used where it was plated along with other plates and at the time of drug treatment, this plate was developed with CTG. The mean of this zero-day control plate was subtracted from each well and then this value normalized to the mean of no cells and DMSO control wells to calculate cell proliferation as a percentage of control. The GI_{50} values were calculated from the normalized cell proliferation data (as a percentage of control) vs. drug concentration graphs using a four-parameter non-linear regression curve fit with the bottom of the curve fixed to 0% (representing no proliferation) using Prism (Graphpad) graphing software. Values below zero represented cytotoxicity.

2-D cell proliferation screening and GI_{50} assays. For the initial screening of the drugs in 2-D, we employed the Incucyte imager to monitor cell confluency in a 96-well format. The harvested cells were seeded at 5,000 cells/well (90 μl) in a 96-well plate (Corning plate #3603) and incubated in the biosafety cabinet for 45 min at room temperature before transferring to an incubator at 37˚C and 5% CO_2 atmosphere. After 24 h, cells were treated manually with compounds diluted into growth media (10 μl) in duplicate wells and incubated in the Incucyte imager for 72 h. The final DMSO in compound treated wells was 0.1% and DMSO was used at 0.1% final concentration for maximum signal control wells. Paclitaxel (0.1 μM) and cycloheximide (10 μM) were used as positive controls. The relative cell growth (increase in confluency) for every well was calculated by first subtracting the confluency data obtained from the first Incucyte read (0 h, representing initial cell area) from the final 72 h read (72 h read-0 h read) to get a net confluency change for every well. This net confluency of every well was then divided by the mean net confluency of the DMSO control well then multiplied by 100 to get relative cell proliferation. This data was plotted using GraphPad Prism and assessed for statistical significance using unpaired t-test to identify active hits, defined as significantly ($P<0.05$) less than 100% of control and having a mean of at least 20% inhibition. For subsequent GI_{50} and cytotoxicity assays, we employed the CellTox Green dye to also measure cytotoxicity along with proliferation in a 384-well format. Hs578T, MDA-MB-231 and SUM-159 cells were seeded at 2,000, 1,500 and 600 cells/well (50 μl/well), respectively, in 384-well plates (Corning, plate # 3764). The cells were incubated for 24 h at 37˚C and 5% CO_2 and then treated with compound using a D300 digital dispenser as triplicates for each compound concentration using an 8-point half-log or two-fold serial dilution scheme starting with 10 μM as the highest concentration. DMSO-only wells were used as a solvent control representing maximal cell proliferation. All wells were adjusted to a final concentration of 0.1% DMSO using the D300. To measure cytotoxic activity, 50 nl of the DNA-binding fluorescent dye CellTox Green stock solution was added to each well immediately after compound addition, resulting in a 1:1,000 dilution from the stock solution provided by the manufacturer. Cells were incubated and monitored for 96 h in the Incucyte as above. To obtain relative cell growth, the confluency data was analyzed by subtracting the initial confluency from the 72 h confluency (72-0 h reads) to get net confluency for each well and then normalizing to the mean net confluency of the DMSO control wells using the same method as above. The GI_{50} values were calculated as above where the bottom was fixed to zero (representing no change in confluency/growth). Relative cytotoxicity values were separately calculated using a published method (11) where the percent green fluorescence confluency values (area of green fluorescence) were divided by the total brightfield confluency (area of cell monolayer), multiplied by 100, where these values were generated by the Incucyte software.

Statistical analysis. In all cases where statistical analysis was performed, an unpaired t-test was employed with n=4 or 6 data points aggregated from replicate experiments where the comparison is between drug treated wells and control wells. An alpha level of 0.05 was used. Error bars on all graphs and variability (±) provided with values represent standard deviation (SD).

Results

NOD screening approach. We sought to identify NODs with the potential to be repurposed for TN-IBC, and TNBC in

general as maintenance therapy. As a first step towards this goal, we utilized the high throughput screening data from Corsello *et al* (12) that is publicly available in the PRISM database (https://depmap.org/repurposing). This group screened a large collection of compounds and drugs using 578 different cancer cell lines by testing drugs against multiple pools of 25 DNA-encoded cell lines mixed in a well in a highly multiplexed cell viability/proliferation assay. We queried this database to obtain all the activity data for non-cancer drugs and approved drugs (Fig. 1). Further selection was applied to those NODs with measurable IC_{50} values (≤10 μM) and with activity in at least three TNBC cell lines, as there were no IBC cell lines in the original screen. These criteria resulted in 100 candidate compounds. From this list, we eliminated actives that were not applicable for direct drug repurposing since they would require steps similar to de novo drug discovery, were redundant or otherwise not of practical use (Fig. 1). Thus, drugs were eliminated that were approved for topical use only, not genuinely approved drugs, highly similar to cancer drugs, prodrugs of other drugs on the list, controlled access drugs and those approved only for animal use. We also chose just one member of highly selective drug classes such as HMG CoA reductase inhibitors (statins). After this further selection process, 48 drugs (Fig. 2) remained on our list and were sourced from vendors for testing in our assays.

We screened these 48 NODs for cytotoxic and anti-proliferative activity against the TN-IBC cell line SUM-149 grown as spheroids. In parallel, we also queried PubMed with the 48 NODs to identify those that have been understudied for TNBC, i.e., ≤1 publication using the terms TNBC and the drug name. The resulting 33 drugs were then screened for activity using two TNBC cell lines, MDA-MB-231 and SUM-159, grown in standard 2-D culture. The 2-D assay was a more rapid screening method enabling the initial screening using two different TNBC cell lines. Since the resultant 2-D data cannot necessarily be directly compared to spheroid data, the hits of highest interest in the 2-D assays were re-tested in spheroid assays as well. Confirmed actives from the SUM-149 and TNBC screens that were also identified as understudied in IBC or TNBC were tested against a panel of TNBC cells grown as spheroids to determine the breadth of activity. Representative images of spheroids for each cell line at treatment time support spheroid integrity (Fig. S1). Prior to treatment, control wells were assessed for viability using CTG and this value was also used to calculate cell proliferation as a percentage of controls.

Initial screens for activity in NOD collection. We screened the collection of 48 NODs at 10 μM drug concentration using the SUM-149 spheroid growth assay in which we measured three parameters as indicators of drug activity (Fig. 2). During the 96 h of drug exposure, we monitored the spheroids with the Incucyte imaging system. After the final reading in the Incucyte imager, we measured total cell viability via ATP detection (CellTiter Glo) (Fig. 2A). We also determined the change in area of the spheroid (Fig. 2B) and cytotoxicity using CellTox Green dye (Fig. 2C) using the Incucyte software. This dye is non-permeant to cells unless the membrane is compromised, upon which the dye binds DNA and its fluorescence increases. Therefore, higher fluorescence indicates cell death. The area of the spheroid was decreased by some drugs and increased by other drugs. An increase in size can be due to cytotoxicity resulting in decreased cell-cell cohesion, reversing a tightly compacted spheroid, resulting in increased total area of the spheroid (13). This phenomenon was observed with the known cytotoxic agent paclitaxel, used as a control in this assay. Paclitaxel generated a mean of 155% change in area compared to control, increased fluorescence and reduced signal in the ATP assay, all consistent with a cytotoxic compound. A decrease in size can be due to decreased cell proliferation during the 96 h assay. For example, this was observed with cycloheximide, a predominately anti-proliferative agent, which decreased mean area, only slightly increased fluorescence and decreased ATP signal. Based on the data, both types of spheroid area changes were observed in this set of compounds. Of the 12 drugs that increased the change in area by ≥125% of control, 9 also displayed an increase in fluorescence in the CellTox Green assay, excluding menadione which displayed autofluorescence and therefore unknown cytotoxicity by this method. Baicalin and menadione, two of the drugs that increased change in area but not fluorescence (baicalin) or were autofluorescent (menadione), also increased the ATP content over DMSO (solvent) control. Thus, these drugs appear to have enhanced proliferation in this cell line. Clofazimine increased the change in area relative to control, but showed no increase in fluorescence, yet clearly inhibited cell proliferation/viability in the ATP content assay. One drug, ivermectin, had no significant effect on the spheroid area, but increased fluorescence and dramatically decreased signal in the ATP assay. If area alone was used in the screen, this drug would have been a false negative and not detected. Thus, use of area alone may result in false positives and false negatives when screening drugs for anti-cancer activity. In another case, niclosamide increased the change in area by a mean of 130%, while the signal in the ATP assay was inhibited by 87%, the latter representing a more robust assay response. In the cytotoxicity assay, 11 drugs (excluding menadione) produced fluorescence >125% of control (DMSO). All these drugs were present as a subset of the ATP assay hits. However, some drugs, e.g., papaverine and spironolactone, were also detected with activity in the ATP assay that showed no increase in fluorescence suggesting they may be only anti-proliferative. Due to the lack of specificity and sensitivity of the area measurement, the robustness of the ATP assay and our interest in identifying both cytotoxic and purely anti-proliferative drugs, the ATP detection assay was used as the primary indicator of activity. Using the ATP assay, we identified drugs that produced a signal significantly lower than control ($P<0.05$) resulting in 22 drugs from this initial screen (Fig. 2A) being selected for confirmatory dose response studies.

In a parallel study, we assessed a subset of 33 drugs (those from the set of 48 drugs with few literature references) for their activity against non-IBC TNBC cell lines SUM-159 and MDA-MB-231 (Fig. 3). A standard 2-D cell culture model was employed, measuring change in percent confluency as a measure of cell growth during the assay using the Incucyte imaging system. The initial confluency at the time of drug treatment (10 μM) was subtracted from the final confluency to get an actual measure of cell proliferation inhibition. Since there

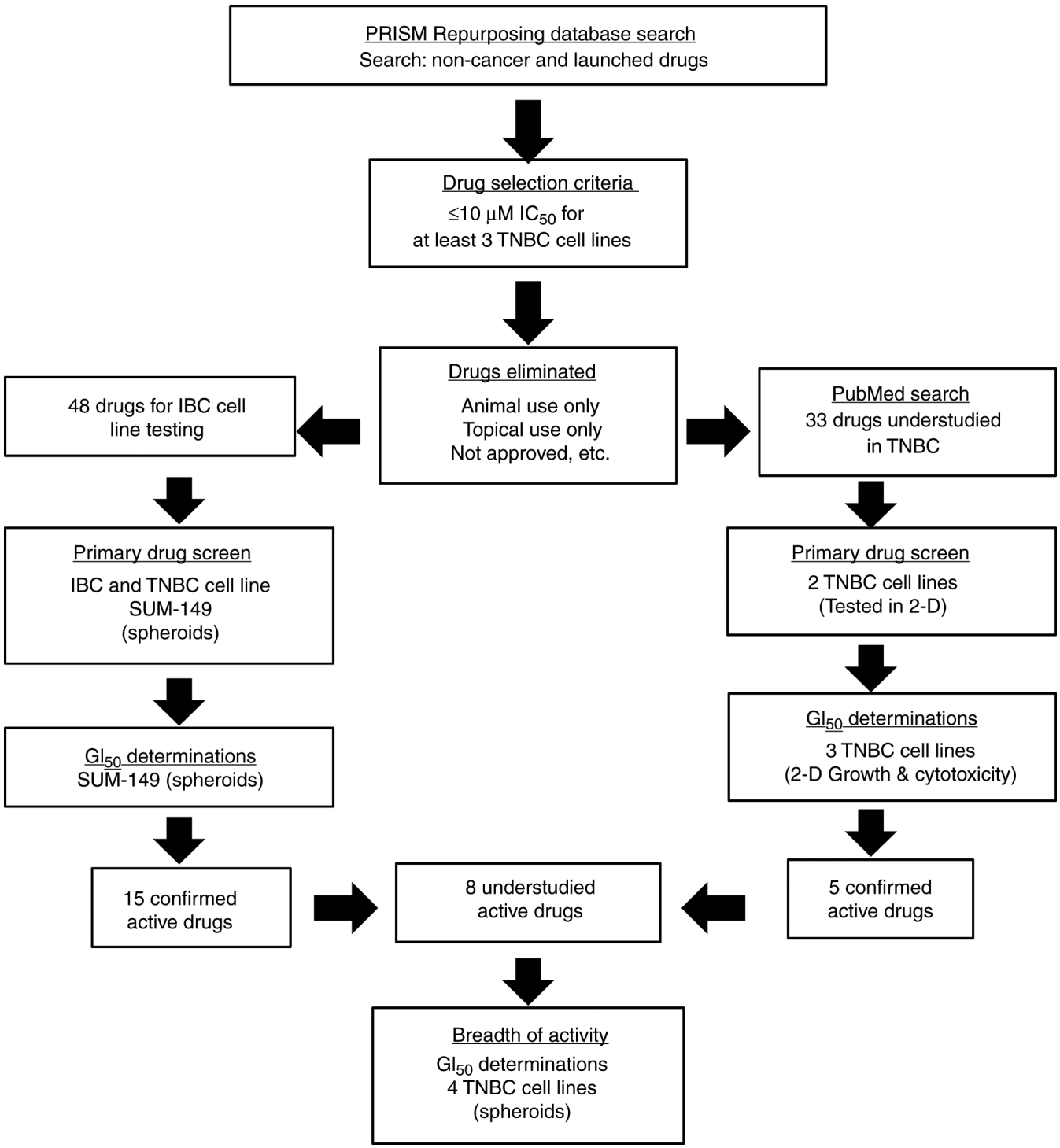

Figure 1. Summary of selection and screening method for identifying drugs with potential for repurposing. A search of the published PRISM database for active drugs in at least three TNBC cell lines resulted in 100 candidates. After drugs were eliminated from this list due to a variety of reasons that reduced potential for rapid repurposing (for example, only approved in animals, only approved for topical use), 48 drugs remained for testing. These were tested in a primary single concentration screen (10 μM) and subsequent actives were then tested in concentration response using the TN-IBC SUM-149 cell line grown as spheroids resulting in 15 confirmed active drugs. A subset of 33 drugs that have been understudied for TNBC were tested in a single concentration (10 μM) screen using two TNBC cell lines in a 2-D cell proliferation assay followed by determination of GI_{50} and cytotoxicity for actives using three TNBC cell lines also grown in 2-D. Five confirmed actives from the 2-D screening were combined with the actives from the SUM-149 screen and assessed for literature reports related to TNBC and IBC resulting in eight understudied drugs. These were profiled for GI_{50} against a total of four TNBC cells lines (including SUM-149) grown as spheroids. TNBC, triple-negative breast cancer; TN-IBC, triple-negative inflammatory breast cancer; 2-D, two-dimension; IBC, inflammatory breast cancer; GI, growth inhibition.

were too many drugs with p≤0.05 that had minimal % inhibition (<10% inhibition) in the 2-D screen, we added a percent inhibition cut-off to the 2-D screen hit criteria. In this screen, 10 actives for SUM-159 and 4 actives for MDA-MB-231 were identified using a cut-off of ≥25% inhibition with P≤0.05 compared to DMSO control (Fig. 3). One drug, mozavaptan, that showed

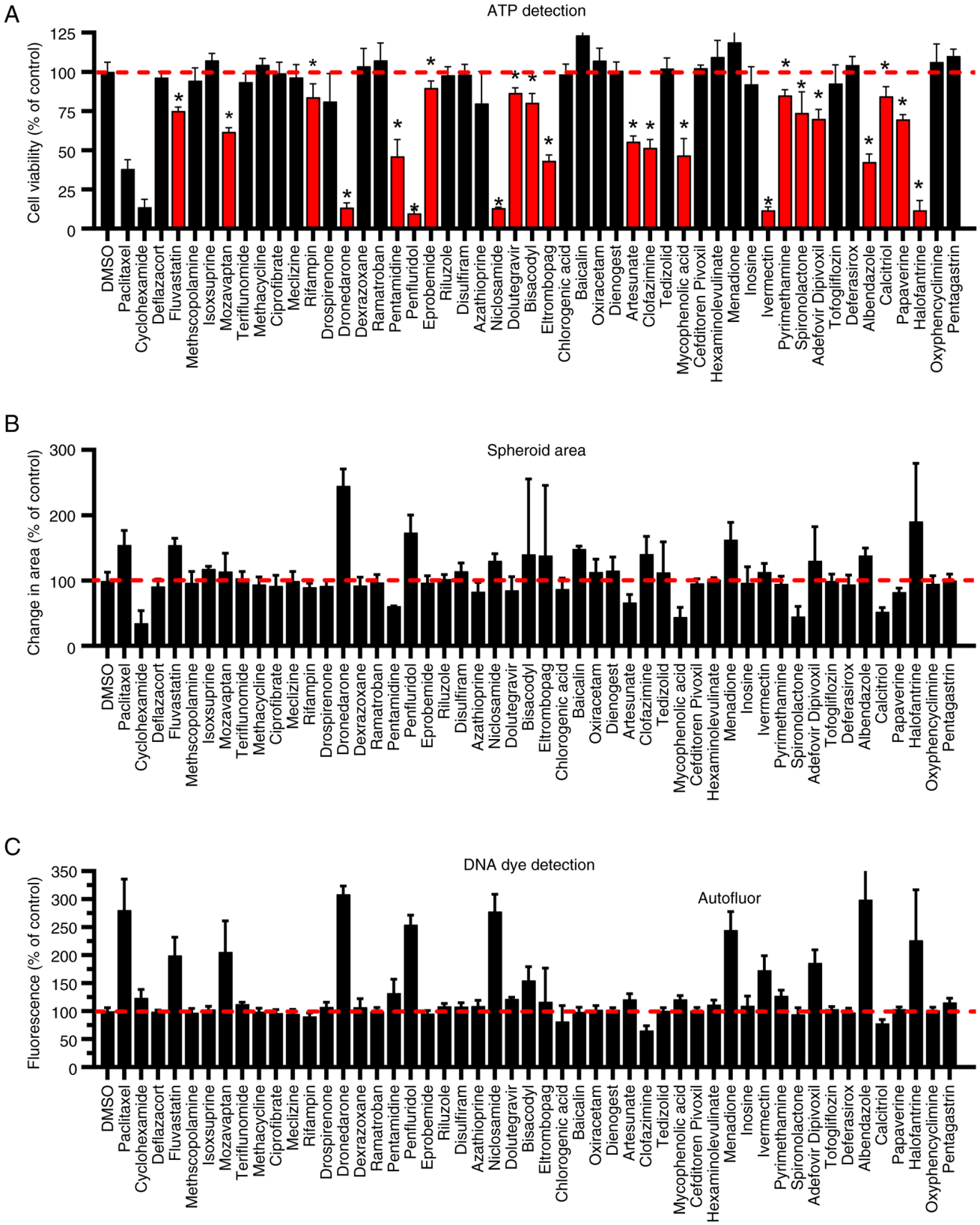

Figure 2. Multiparametric screen of selected NODs for activity against TN-IBC cell line SUM-149 grown in spheroid culture. A total of 48 drugs (as indicated on the y-axis) were tested at 10 μM against SUM-149 grown as spheroids. DMSO wells were solvent control wells used to normalize the data and paclitaxel and cycloheximide were used as control inhibitors. (A) After 96 h of drug exposure, CellTiter Glo was used to determine ATP levels as a reflection of cell viability, calculated as percentage of controls. Red bars represent drugs that had significantly reduced cell viability compared to DMSO control using unpaired t-test and therefore were selected for GI_{50} determinations ($^{*}P<0.05$ compared to DMSO). (B) The change in spheroid area between 0 and 96 h was calculated for each drug as a percentage of DMSO control. (C) Non-permeable CellTox Green dye was used to detect free DNA by measuring the total green fluorescence of the well and normalizing it to controls. Normalized data >100% was indicative of cytotoxicity. The drug marked 'Autofluor' showed fluorescence at time 0 indicating that the fluorescence was high due to autofluorescence of the drug. Screening data shown represents the mean ± standard deviation of the aggregated normalized data from n=2 or 3 independent experiments where each experiment employed duplicate technical replicates. NOD, non-oncology drug; TN-IBC, triple-negative inflammatory breast cancer; DMSO, dimethyl sulfoxide.

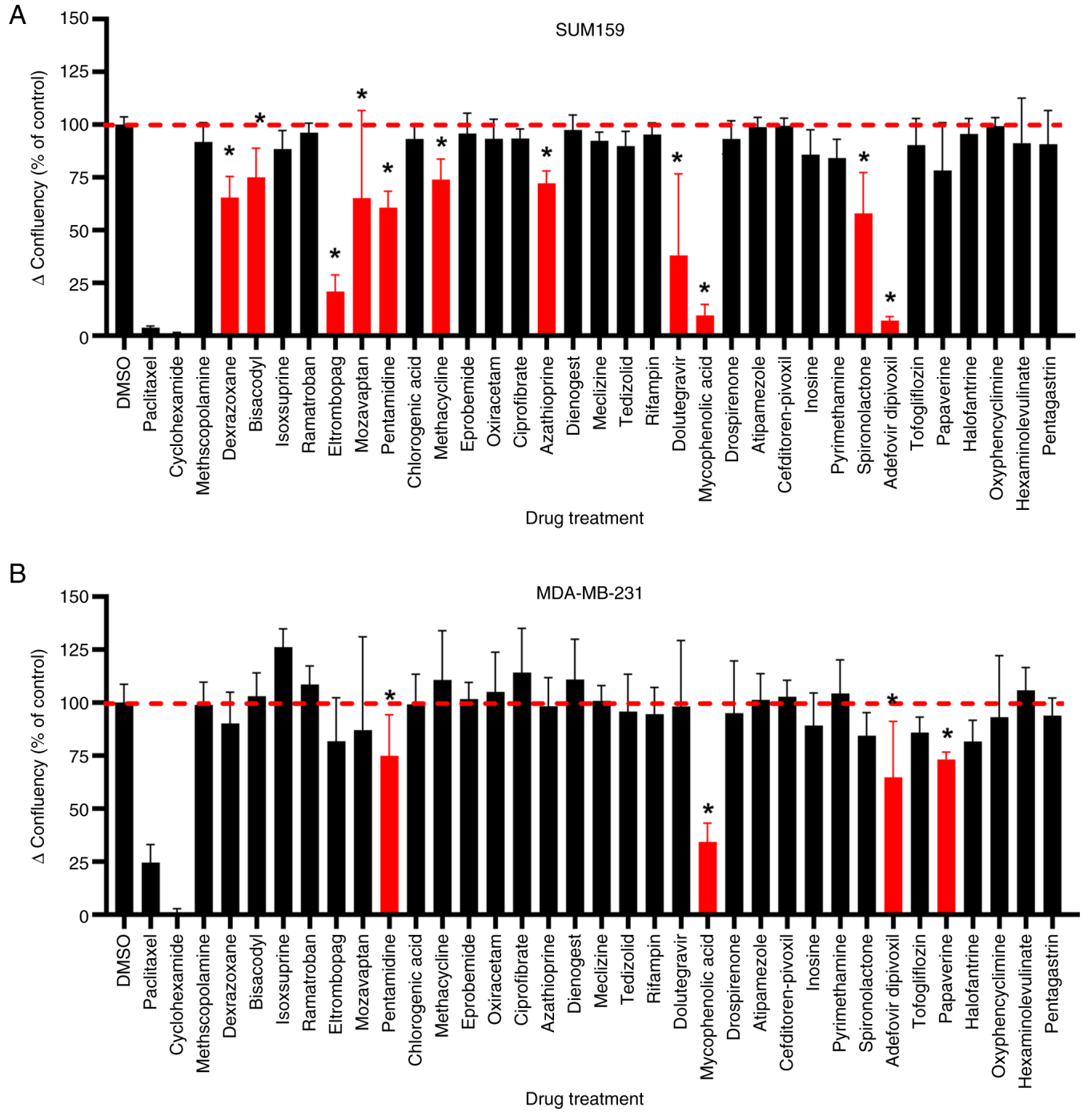

Figure 3. 2-D screen of selected NODs for activity against two TNBC cell lines. 32 drugs (as indicated on the y-axis) were tested at 10 μM against (A) SUM-159 and (B) MDA-MB-231 grown in 2-D. Change in monolayer confluency between 0 and 72 h was calculated for each drug as a percentage of DMSO control. DMSO wells were solvent control wells used to normalize the data and paclitaxel and cycloheximide were used as control inhibitors. Red bars represent drugs that had significantly reduced cell viability compared to DMSO control using unpaired t-test and displayed ≥20% inhibition (*P<0.05 compared to DMSO). These active drugs were selected for GI_{50} determinations. Screening data shown represents the mean ± standard deviation of the aggregated normalized data from n=3 independent experiments where each experiment employed duplicate technical replicates. NOD, non-oncology drug; TNBC, triple-negative breast cancer; DMSO, dimethyl sulfoxide.

unusually high variability in activity against SUM-159, was also re-tested in potency assays. Due to the inclusion of mozavaptan and significant overlap in actives, the screen resulted in 12 unique drugs selected for confirmation assays.

Confirmation concentration response assays. The active drugs from the SUM-149 spheroid screen were tested in concentration response assays using the same format, except that only the ATP assay was used as a measure of cell viability and proliferation. An initial measure of luminescence ('day 0' signal) allowed for subtraction of the signal derived from plated cells and therefore, enabled the plotting of spheroid growth relative to controls to derive a GI_{50}. Thus, this method allowed detection of both cytostasis and cytotoxicity since the normalized 0 signal represents no cell growth and negative values indicate cytotoxicity. GI_{50} was determined, rather than simple

Table I. GI_{50} values in the SUM-149 spheroid assay and pharmacological data for identified drugs.

Drug	GI_{50} (μM)[a]	SD (μM)	GI_{50}:C_{max}	C_{max}[b] (μM)	Drug class or MOA	Approved indication
Adefovir-dipivoxil	4.8	0.2	18.5	0.26	Nucleotide analog reverse transcriptase inhibitor	Hepatitis B
Albendazole	1.4	0.3	0.3	5.70	Tubulin inhibitor	Parasitic worm infections
Artesunate	0.7	0.1	0.1	8.00	Generates free radicals	Malaria
Bisacodyl	6.6	2.7	26.4	0.25[b]	Stimulates adenylate cyclase	Constipation
Clofazimine	6.6	2.4	8.6	0.77	Acts at bacterial membranes	Leprosy
Dolutegravir	>40[c]	-	NA	6.30	Integrase inhibitor	HIV-1
Dronedarone	5.7	0.6	19.0	0.30	Multichannel blocker	Atrial fibrillation
Eltrombopag	14.0[d]	6.2	1.0	14.00	Thrombopoietin receptor agonist	Thrombocytopenia
Halofantrine	7.1	3.1	10.3	0.69	Targets ferritoporphyrin IX	Malaria
Ivermectin	2.9	0.5	36.3	0.08	Chloride ion channels	Multiple parasites
Mozavaptan	>10[e]	-	NA	Unk	Vasopressin receptor antagonist	Hyponatremia[f]
Mycophenolic acid	0.5	0.1	0.01	78.00	IMPDH inhibitor	Immunosuppressant
Niclosamide	0.2	0.02	0.6	0.27	Uncoupling of electron transport	Tapeworm infections[g]
Papaverine	7.1	2.2	2.4	2.90	Nonxanthine PDE inhibitor	Myocardial infarction/ angina
Penfluridol	2.1	0.1	42.0	0.05	Dopamine receptor blocker	Antipsychotic[h]
Pentamidine	6.7	2.1	10.6	0.63	Unknown	Pneumocystis pneumonia
Spironolactone	3.5	0.1	10.0	0.35	MR antagonist	Hypertension, heart failure

[a]Highest concentration tested was 10 μM, except for dolutegravir and eltrombobag which were tested at 40 μM high concentration, as indicated; GI_{50} values are the mean of n≥3 independent experiments. [b]C_{max} values were obtained from literature (24-37). Plasma concentration of bisacodyl and free metabolite bis-(p-hydroxyphenyl)-pyridyl-2-methane (BHPM) are below detection (<1 ng/ml), therefore the concentration provided is that of BHPM glucuronides. [c]Variable responses, tested at high concentration of 40 μM, 0.4% DMSO. [d]Mean of dose response curves starting at high concentration of 10 (n=3) and 40 μM (n=4), 0.1 and 0.4% DMSO, respectively. [e]Variable responses: 4 to >10 μM. [f]Not approved by FDA; approved in Japan. [g]Not currently on the market in USA. [h]Not approved by FDA; marketed in other countries. IMPDH, inosine-5'-monophosphate dehydrogenase; PDE, phosphodiesterase; MR, mineralocorticoid receptor; MOA, mechanism of action; NA, not applicable; Unk, unknown.

IC_{50}, since our interest was to identify potential maintenance therapy, including drugs that only slowed re-growth of cancer cells after standard of care treatment. Since NODs were not originally designed as cytotoxic chemotherapy agents, the expectation was that at clinical doses, many of these NODs may only inhibit cell growth. Thus, NODs that are purely anti-proliferative would still be of interest and we wanted to accurately quantify this anti-proliferative activity. 15 drugs had calculable GI_{50} values (reached at least 50% inhibition) (Fig. 4 and Table I). The GI_{50} values ranged from 0.17 to 14 μM and originated from various drug classes and approved indications (Table I). At the higher potency end of this collection of drugs (<2 μM GI_{50}), the anti-cancer activity of niclosamide (GI_{50}=0.17 μM), mycophenolic acid (GI_{50}=0.51 μM), artesunate (GI_{50}=0.69) and albendazole (GI_{50}=1.4 μM) have all been extensively described (14). In addition to TNBC, niclosamide has also been shown by others to have activity against SUM-149 (15-17). While the activity of artesunate and albendazole has been described for TNBC cell lines (18-21), their activity against SUM-149 (or other IBC cell lines) does not appear to have been previously reported.

The active drugs from the TNBC 2-D screen were tested in concentration response assays using the same format as the initial screen, except that CellTox Green dye was used as a measure of cytotoxicity, while confluency was used to measure cell proliferation. All the actives were tested against three TNBC cell lines: SUM-159, MDA-MB-231 and Hs578T. Five drugs had confirmed GI_{50} potencies of <10 μM for at least one cell line: adefovir, eltrombopag, mozavaptan, mycophenolic acid and pentamidine (Fig. 5 and Table II). Halofantrine was a sixth drug that was also tested in this 2-D panel since it had borderline activity against MDA-MB-231 and activity in the spheroid screen. Mozavaptan was the only drug in this set that had activity against all three cell lines with mean GI_{50} values of 2.2 to 4.6 μM. MDA-MB-231 appeared to be more drug resistant in general within this panel than the other two cell lines since only two of these drugs had calculatable GI_{50}s against this cell line. The most potent drugs were adefovir (mean GI_{50}=1.2, 3.3 and >10 μM) and mycophenolic acid (mean GI_{50}=0.5, 3.1 and >10 μM). Adefovir showed cytotoxicity only against SUM-159. Mycophenolic acid has been extensively studied for its anti-cancer activity,

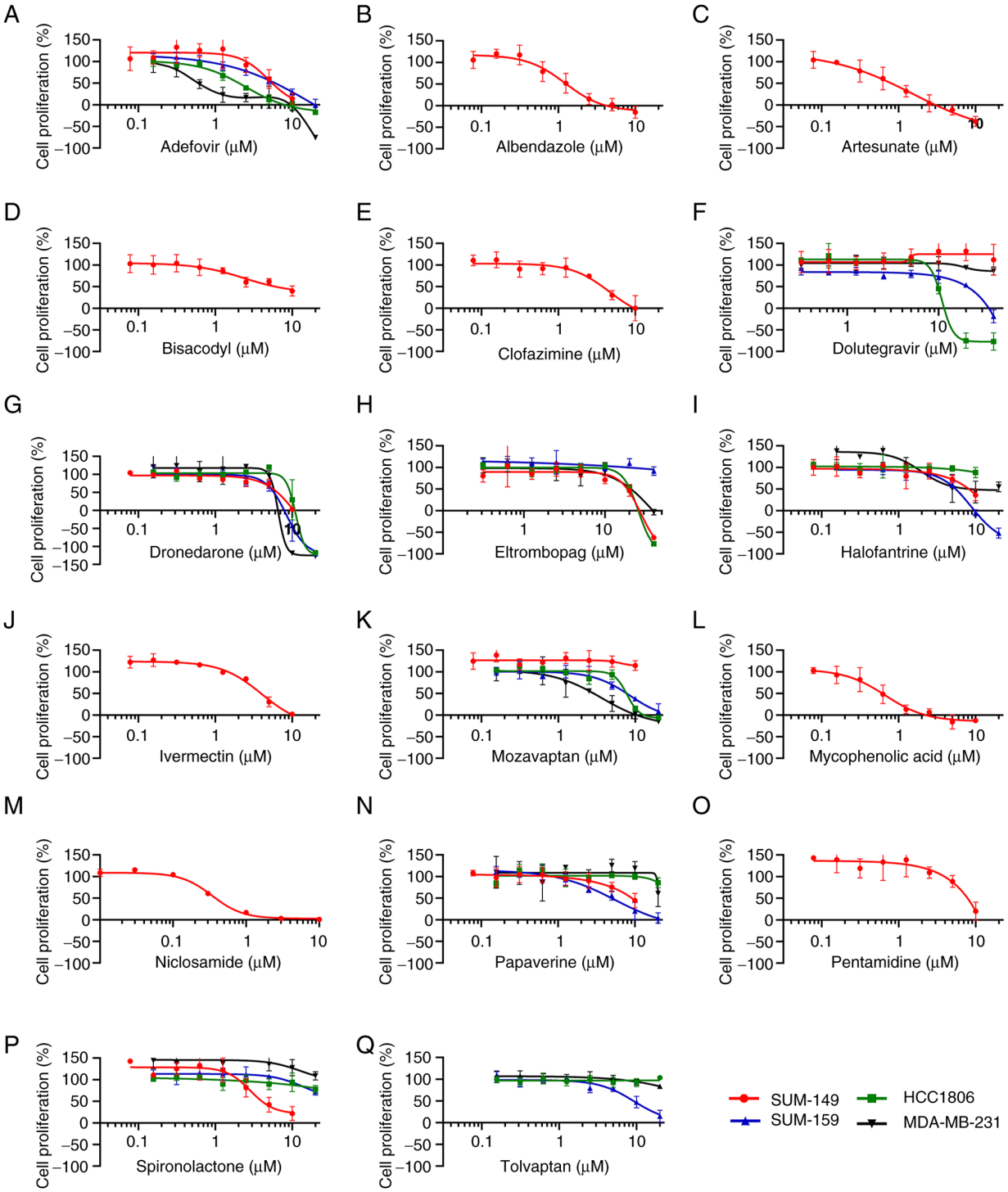

Figure 4. GI_{50} determinations for active drugs against SUM-149 and a panel of other TNBC cell lines grown as spheroids. Relative cell proliferation (as a percentage of controls) was determined in response to the indicated concentrations of drugs tested against SUM-149. Selected compounds were also profiled with an additional three TNBC cell lines, SUM-159, HCC1806 and MDA-MB-231, as indicated. The concentration response data was plotted for (A) adefovir, (B) albendazole, (C) artesunate, (D) bisacodyl, (E) clofazimine, (F) dolutegravir, (G) dronedarone, (H) eltrombopag, (I) halofantrine, (J) ivermectin, (K) mozavaptan, (L) mycophenolic acid, (M) niclosamide, (N) papaverine, (O) pentamidine, (P) spironolactone and (Q) tolvaptan. All cell lines were grown in spheroid form for this assay with 96 h drug treatment followed by viable cell number assessed by CellTiter Glo. Relative cell proliferation (as opposed to total cells) was calculated by subtracting mean 0-day plate values from all wells and normalizing to controls such that a 0 value indicated no cell proliferation during the course of the assay (same number of viable cells as on day of treatment), while negative values indicated cytotoxicity (fewer viable cells than on day of drug treatment). Data shown are representative of n≥3 independent experiments and the data points and error bars represent the mean ± standard deviation of triplicate technical replicates. GI, growth inhibition; TNBC, triple-negative breast cancer.

including against TNBC cell line MDA-MB-231 (22,23). However, no studies to date have reported its activity against SUM-149 or other IBC cell lines. A measure of cytotoxicity was calculated by dividing the area of green fluorescence (from the CellTox Green dye) by the area of confluency (from the brightfield image) (Fig. 5). Mozavaptan was the only drug

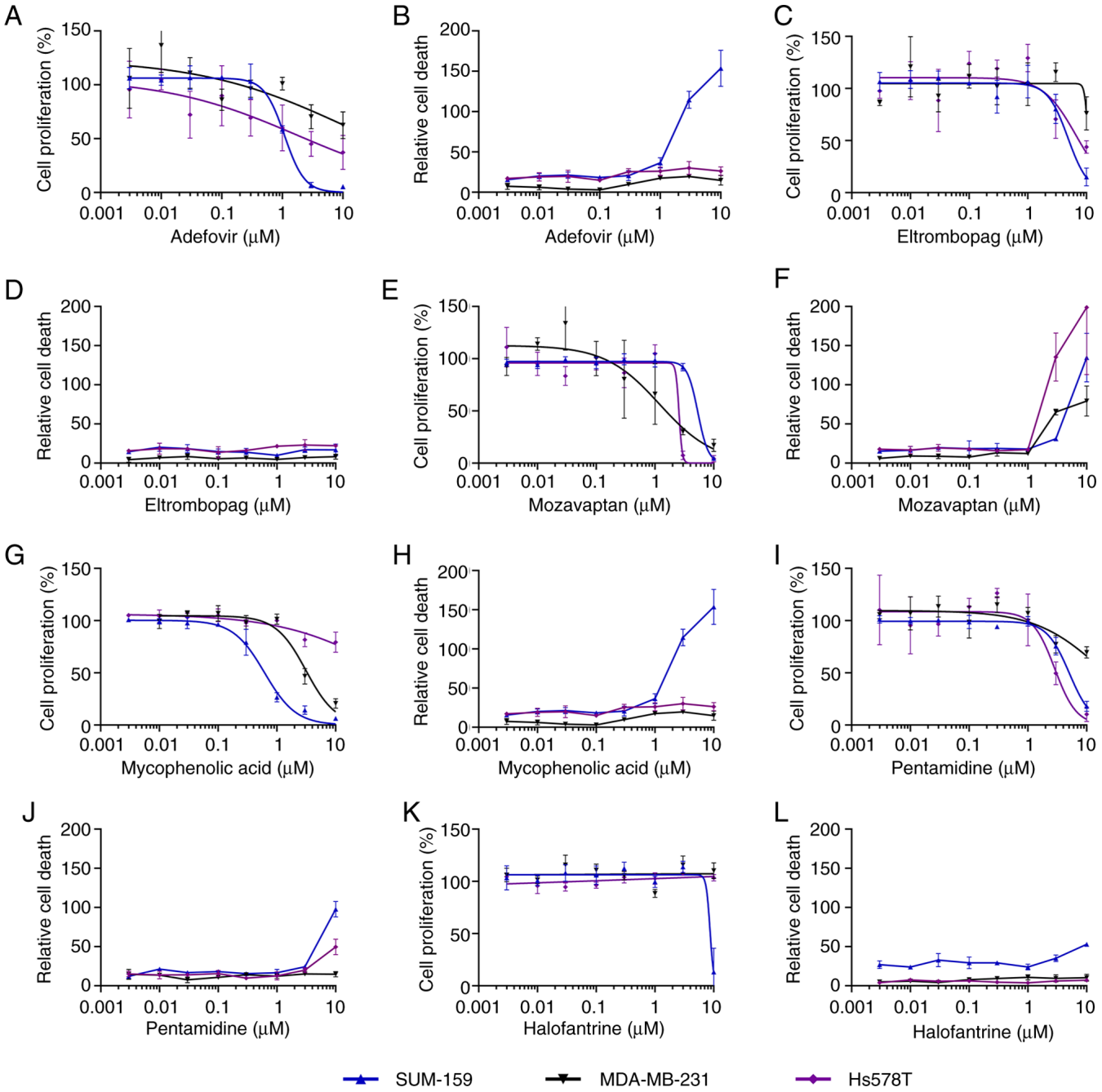

Figure 5. GI_{50} determination of active drugs from 2-D screen against a panel of three TNBC cell lines. Relative cell proliferation (as a percentage of controls) and cytotoxicity was determined in response to the indicated concentrations of drugs tested against SUM-159, HCC1806 and MDA-MB-231, as indicated. All cell lines were grown in 2-D. Immediately after drug treatment, confluency and CellTox Green dye fluorescence (cytotoxicity) was monitored for 72 h with the Incucyte. Relative cell proliferation was calculated by subtracting the initial confluency (based the first read) from the final confluency measurement for each well and normalized to controls. Therefore, a 0% value indicates no change in confluency compared to the start of the assay. Relative cell death after 72 h was calculated by dividing the area of green dye fluorescence by the total confluency area (based on brightfield imaging) and multiplying by 100. Separate plots are provided for cell proliferation and cytotoxicity for (A and B, respectively) adefovir, (C and D, respectively) eltrombopag, (E and F, respectively) mozavaptan, (G and H, respectively) mycophenolic acid, (I and J, respectively) pentamidine and (K and L, respectively) halofantrine. Data shown are representative of n≥3 independent experiments and the data points and error bars represent the mean ± standard deviation of triplicate technical replicates. GI, growth inhibition; TNBC, triple-negative breast cancer; 2-D, two-dimension.

that was cytotoxic against all three cell lines where it generated cytotoxicity at concentrations above 1 μM. In contrast to mozavaptan, the other drugs in this set that showed some cytotoxicity only had cytotoxic activity against one cell line (e.g. mycophenolic acid and adefovir) or weak cytotoxic activity (only at 10 μM) against one or two cell lines (e.g. pentamidine and halofantrine). Eltrombopag did not show cytotoxicity against any of the cell lines and thus appeared to be purely anti-proliferative under these 2-D conditions. Adefovir and mycophenolic acid were only cytotoxic for SUM-159 at 3 μM and above.

Activity of understudied NODs in a panel of TNBC cell lines. Since SUM-149 is the only commercially available TN-IBC

Table II. GI_{50} for drugs identified in 2-D cell culture screen.

Cell line	SUM-159		MDA-MB-231		Hs578T	
Drug	GI_{50} (μM)[a]	SD	GI_{50} (μM)[a]	SD	GI_{50} (μM)[a]	SD
Adefovir dipivoxil	1.2	0.3	>10	-	3.3[b]	1.5
Eltrombopag	8.1	1.0	>10	-	5.3[b]	1.3
Halofantrine	7.6	1.1	>10	-	>10	-
Mozavaptan	4.6	0.5	2.2	0.7	2.7	0.7
Mycophenolic acid	0.5	0.1	3.1	0.3	>10	-
Pentamidine	7.4	1.8	>10[c]	-	2.0[b]	0.9

[a]Highest concentration tested was 10 μM; GI_{50} values are the mean of n≥3 independent experiments except where indicated. [b]Mean of n=2 independent experiments. [c]One value 7.2 μM.

Table III. Anti-proliferative activity of selected drugs in a panel of cell lines grown as spheroids.

Cell line	SUM-149		HCC-1806		SUM-159		MDA-MB-231	
Drug	GI_{50} (μM)[a]	SD	GI_{50} (μM)	SD	GI_{50} (μM)	SD	GI_{50} (μM)	SD
Adefovir	4.8	0.2	2.0	0.6	4.2	1.5	1.3	1.0
Dolutegravir	>40[b]	-	16.0	11.0	27	7.5	>40	-
Dronedarone	5.7	0.6	8.1	2.6	5.3	0.3	5.8	3.9
Eltrombopag	14.0	6.2	16.8	5.2	>40	-	16.8	6.1
Halofantrine	7.1	3.1	>20[c]	-	5.1	0.03	10.2	7.2
Mozavaptan	>10[d]	-	6.7	0.7	7.6	2.0	3.3	0.7
Papaverine	7.1	2.2	>20[c]	-	4.2	0.3	>20[c]	-
Spironolactone	3.5	0.05	>20	-	>20[c]	-	>20[c]	-
Tolvaptan	NT	-	>20	-	12.2	6.2	>20	-

[a]Highest concentration tested was 10 μM (SUM-149) or 20 μM (all other cell lines), except dolutegravir and eltrombopag tested at a high of 40 μM; GI_{50} values are the mean of n≥3 independent experiments. [b]Variable responses. [c]One value was >12 μM. [d]Variable responses: 4 to >10 μM. NT, not tested.

cell line, we were unable to test the active hits against other TN-IBC cell lines. Therefore, we sought to test understudied NODs from the SUM-149 screen against standard TNBC cell lines to assess the breadth of activity. Of the 15 drugs that were confirmed in the SUM-149 screen, 7 of them were assessed to be understudied in TN-IBC/TNBC based on PubMed literature searches. Similarly, 5 of the hits in the 2-D screen with TNBC cell lines had few studies related to their activity in TNBC. We combined these sets of drugs, resulting in 8 unique understudied drugs, due to high overlap in the lists. Only mozavaptan was a novel hit in the 2-D screen compared to the SUM-149 screen hits. Dolutegravir was understudied in the literature but was highly variable in the SUM-149 potency assays for unknown reasons, so we included it for testing against this panel. We tested these eight drugs in concentration response against TNBC cell lines SUM-159, HCC1806 and MDA-MB-231 grown in the spheroid assay format with ATP detection as the measure of cell viability and proliferation (Fig. 4, Table III and Fig. 6A). Since we performed a 'Day 0' plate to obtain the signal for the initial cell number at the time of drug treatment, a negative cell proliferation value at the end of drug treatment indicated fewer viable cells, i.e., cytotoxicity. Hs578T failed to proliferate in the spheroid growth conditions employed, so we used HCC1806 in its place. Eltrombopag and dolutegravir were tested at higher max concentration (40 μM) due to their higher C_{max} values. Adefovir, an anti-hepatitis B antiviral drug, and dronedarone, a multi-channel blocker for atrial fibrillation, were the only drugs in this selected drug panel to inhibit all four cell lines with a calculatable GI_{50} value. Adefovir produced mean GI_{50} values ranging from 1.3 to 4.8 μM and it appeared to be cytotoxic for MDA-MB-231 at 20 μM, but not for the other cell lines. Dronedarone produced GI_{50} values in the range of 5.3 to 8.1 μM and was cytotoxic at higher concentrations across the cell lines. Three of the drugs had measurable GI_{50} values in three of the four cell lines. These drugs and their GI_{50}s for SUM-149, HCC1806, SUM-159 and MDA-MB-231, respectively, included eltrombopag (GI_{50}=14, 16.8, >40 and 16.8 μM), halofantrine (GI_{50}=7.1, >20, 5.1, 10.2 μM) and mozavaptan (GI_{50}=>10, 6.7, 7.6, 3.3 μM). Since mozavaptan is a vasopressin receptor antagonist, we sought

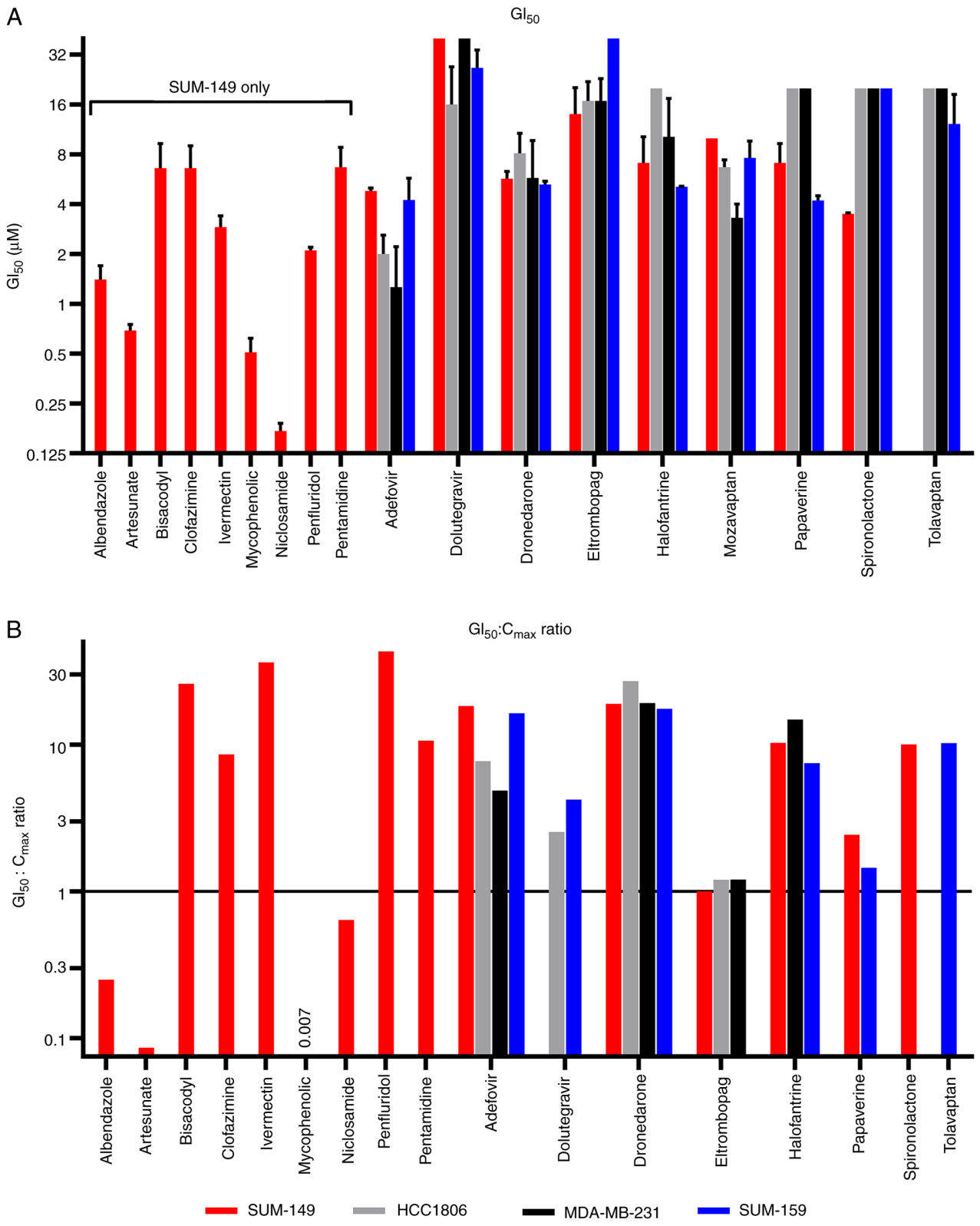

Figure 6. Graphical representations of mean GI_{50} values and GI_{50}:C_{max} ratios for active drugs. The GI_{50} data from Tables I and III were represented as bar graphs. (A) Mean GI_{50} values of compounds tested only against SUM-149 (as indicated) or against all four cell lines were plotted. No error bars indicate that the GI_{50} is greater than the highest concentration tested and thus shown as equal to that high concentration (i.e., GI_{50} of >20 μM is indicated by a bar at 20 μM without error bars). (B) The mean GI_{50} values were divided by the C_{max} values from Table I and plotted for each indicated drug. The ratio of one is indicated with a horizontal black line. GI, growth inhibition; C_{max}, maximal concentration.

to test another member of this class, tolvaptan, for its activity (Table III, Fig. 4Q). Tolvaptan only had weak activity against SUM-159 (GI_{50}=12 μM) out of the three TNBC cell lines tested. Eltrombopag was clearly cytotoxic only at 40 μM for two (SUM149 and HCC1806) of the three sensitive cell lines. Papaverine had activity against SUM-149 (GI_{50}=7.1 μM)

and SUM-159 (4.2 μM), but minimal activity (GI_{50} >20 μM) against the other two cell lines. Dolutegravir exhibited activity only against SUM-149 and HCC1806 and showed notable cytotoxicity for HCC1806 at concentrations of 20 μM and above. Spironolactone was the only drug in this subset of drugs that was selective for SUM-149 (GI_{50}=3.5 μM), with no activity against the other three cell lines.

GI_{50} values are more informative when viewed relative to the maximal concentration (C_{max}) achievable at clinical doses in humans. We obtained C_{max} values for the identified drugs using published C_{max} values from human clinical studies (Table I) (24-37). By comparing the GI_{50} values from the SUM-149 data to the C_{max} values (Table I and Fig. 6B), 9 drugs had GI_{50} values that were 10-fold or more higher than the C_{max} (GI_{50}:C_{max} ratio of ≥10). One drug, mozavaptan, had no published C_{max} data. However, there were 6 drugs that had GI_{50} values that ranged from approximately twice their C_{max} to 153-fold lower than their C_{max}. These drugs and their approximate GI_{50}:C_{max} ratio included the following: albendazole (GI_{50}:C_{max}=0.3), artesunate (GI_{50}:C_{max}=0.09), mycophenolic acid (GI_{50}:C_{max}=0.007), Niclosamide (GI_{50}:C_{max}=0.6), eltrombopag (GI_{50}:C_{max}=1) and papaverine (GI_{50}:C_{max}=2). Eltrombopag and papaverine had similar relative potencies (GI_{50}:C_{max} ratios) for the other cell lines that were sensitive to them. Adefovir had a Cmax of 0.2 μM and a GI_{50}:C_{max} of 18 for SUM-149. However, in MDA-MB-231 cells, adefovir produced a GI_{50} of 1.3 μM which is only 5-fold above C_{max}. Interestingly, this drug was inactive (>10 μM GI_{50}) in the 2-D potency assay with MDA-MB-231. This contrasts with the results obtained with the same drug in SUM-159, where the potency shifted almost 4-fold, indicating a less sensitive response in the spheroid assay, suggesting a shift in potency due to the spheroid culture conditions. It has been well established that compound potency shifts can frequently happen when comparing 2-D and 3-D cell culture, including many instances when lower potency is observed in the 3-D culture (38,39).

In sum, we screened a collection of 48 NODs identified through a published database for anti-proliferative activity against the IBC cell line SUM-149 grown in spheroid format. We identified 15 NODs with activity against SUM-149. A subset of 33 NODs was also screened using two TNBC cell lines grown in 2-D culture resulting in the identification of six drugs. There was complete overlap in these sets of drugs, except for mozavaptan which was only identified in the TNBC screen. In the SUM-149 assay, the most potent drugs (<1 μM GI_{50}) were artesunate, mycophenolic acid, and niclosamide. Six of these drugs active against SUM-149 (albendazole, artesunate, mycophenolic acid, niclosamide, eltrombopag and papaverine) have potentially clinically relevant GI_{50}:C_{max} ratios of ≤2. Eight drugs were further tested against a panel of three non-IBC TNBC cell lines grown in spheroid format. Selectivity varied from two drugs (adefovir and dronedarone), which had activity against all four cell lines, to one (spironolactone), which had activity only against SUM-149. Eltrombopag and papaverine were identified as having newly discovered activity against SUM-149, and we expanded their activity profiling to multiple TNBC cell lines. In addition, the eltrombopag and papaverine had GI_{50}:C_{max} ratios of 1 and 2, respectively, indicating that they could reach therapeutically relevant drug levels *in vivo* for anti-cancer treatment.

Discussion

In this report, we screened a collection of NODs based on a published database to identify NODs with activity against TN-IBC and/or TNBC. Using the TN-IBC cell line SUM-149, we identified 15 drugs with calculable GI_{50} values against this cell line grown in spheroid form. In a parallel screening approach, we tested a subset of these NODs for activity against two other TNBC cell lines grown in 2-D. This second approach resulted in a list of active drugs that overlapped with the SUM-149 hits, except for mozavaptan which was uniquely active against SUM-149. Rather than just using the absolute GI_{50} for assessing their potential against TN-IBC, we also assessed these drugs in terms of their potency (GI_{50}) relative to their C_{max} reported in human studies. Many of these drugs turned out to be well-known NODs that have many reports of their anti-cancer activity. For example, the well-studied NODs, albendazole (anti-parasitic), artesunate (anti-malarial), niclosamide (for tapeworm infections) and mycophenolic acid (immunosuppressant) have been extensively reported to have anti-cancer activity against multiple types of cancers (10,14). These drugs also have C_{max} values in humans that are above the GI_{50} reported here for SUM149 and hence may have activity against IBC in patients. From the two screening approaches, eight of these NODs were identified as being less studied in TNBC, and so we tested these drugs against a panel of other TNBC cell lines grown in spheroid format. Only two drugs generated calculable GI_{50} values in all four cell lines: adefovir (antiviral) and dronedarone (multichannel blocker for atrial fibrillation). However, these drugs also had GI_{50}:C_{max} ratios that were high, at approximately 5- to 30-fold, and raises the question of how effective they would be at clinical doses. The sensitivity to adefovir varied between cell lines with MDA-MB-231 being the most sensitive with a GI_{50} of 5-fold above $C_{max.}$ Halofantrine (antimalarial) had activity in 3 of 4 cell lines, but the GI_{50}:C_{max} values were all over 7-fold. Dolutegravir (HIV drug) had activity against two cell lines (but not SUM-149) with a GI_{50}:C_{max} of ~3-4-fold. While this drug was reported to inhibit proliferation of BT-20, a TNBC cell line, it was also found to increase metastasis in the 4T1 (mouse TNBC cell line) xenograft model (40). Two drugs, eltrombopag and papaverine had GI_{50}: C_{max} ratios of 1 to 2 in sensitive cell lines. These drugs have not been previously reported to have activity in an IBC cell line.

A limitation of this study was the reliance on SUM-149 as the sole TN-IBC model, since the observed drug activity could be due to cell line-specific effects and not generalizable to most TN-IBC. Hence, these drugs should be tested against other TN-IBC cell lines. Suggestive evidence against unique SUM-149 effects is that most of the drugs active against SUM-149 were also active against other TNBC cell lines. Another limitation of this study was that the simple spheroid model does not fully recapitulate IBC-specific *in vivo* mechanisms such as tumor emboli formation and lymphangiogenesis. The use of Cmax in our data analysis also has its limitations. Protein binding of drugs in serum may alter the concentration of free drug *in vivo* compared to 10% serum used in our *in vitro* studies. In addition, the Cmax only reflects the concentration achieved in blood, while the degree of tissue penetration may alter the concentration of drug experienced

by the tumor. In addition, chronic dosing may increase the concentration of drug in the serum and tumor. Thus, our use of Cmax in assessing the drugs is only a rough guideline, but an improvement over ignoring the realities of clinically achievable *in vivo* drug concentrations and how it dramatically varies between drugs. The spheroids were not characterized for properties described in the literature for spheroid culture, including hypoxia, proliferation gradients and necrotic centers. Therefore, validation of these properties in our assays needs to be confirmed in future work.

Eltrombopag is a thrombopoietin receptor (TPOR) agonist that is approved for treatment of thrombocytopenia. Despite this originally designated target, eltrombopag has been experimentally demonstrated to bind to multiple targets including proteins such as BAK (41), TFEB (42) and Syndecan-4 (43). Eltrombopag has also been reported to directly inhibit BAX and prevent cell death (44). It has been reported to bind double-stranded DNA (45), chelate iron (46-48) and have anticancer activity in multiple cell lines from many different tissue origins (49-52). Despite low or undetectable TPOR in most tissues, eltrombopag has been reported to inhibit cell growth in multiple different cancer cell lines including breast cancer cell lines MCF-7, BT-474 and TNBC cell line HCC1937 (50). Eltrombopag has been reported as an inhibitor of the mRNA-binding protein, HuR (human antigen R), which has been associated with poor prognosis in multiple cancers (51,53,54). In Zhu *et al* (53), eltrombopag also inhibited cell proliferation in multiple cancer cell lines, but no human TNBC cell lines were tested. In their work, using the murine TNBC cell line 4T1, eltrombopag had an *in vitro* IC_{50} of 13.5 μM, similar to our data with human TN-IBC/TNBC cell lines. In a mouse allograft model using 4T1, eltrombopag also had *in vivo* activity where it inhibited tumor growth and metastasis and displayed anti-angiogenesis activity (53,54). Our data adds to this body of research since we demonstrated that eltrombopag had activity in 3 of 4 human TNBC cell lines grown in spheroid form, including a TN-IBC cell line, with potencies similar to its C_{max}. At the highest concentration tested, 40 μM, eltrombopag was cytotoxic in two of the four cell lines. The weak potency of eltrombopag against SUM-159 (GI_{50} >40 μM) also suggests some TNBC cancers may be resistant to this drug. According to RNAseq data accessed through the Depmap portal (https://depmap.org), the expression level of the gene for TPOR (MPL) is very low (close to undetectable) in all four cell lines used in this study, which is consistent with undetectable expression of MPL mRNA in 118 advanced or metastatic breast cancer samples from patients (50). However, TPOR expression in the cell lines used in this study needs to be confirmed in future studies. Due to the many off-target activities that have been ascribed to eltrombopag, it is not clear which mechanism was producing the observed activity in our assays. The C_{max} of 14 μM cited herein was the result of a single dose of 50 mg of eltrombopag in healthy adults (35). Another study dosed healthy adults with up to 75 mg of eltrombopag per day for 10 days and concluded that there were no significant adverse effects compared to placebo (55). In this study, the 30-, 50-, and 75-mg dose levels resulted in mean increases in platelet counts of 24.1, 42.9, and 50.4%, respectively. The normal platelet count in adults ranges from 150,000 to 450,000 platelets per microliter, with counts exceeding 450,000 platelets per microliter defined as thrombocytosis (56). Thus, depending on an individual's baseline platelet count, even a 50% increase in platelet count caused by eltrombopag treatment may still be within normal range. A long-term study in patients with chronic immune thrombocytopenia taking eltrombopag for up to 3 years (median daily dosing of 51.5 mg) found that the most common adverse events were headache, nasopharyngitis, upper respiratory tract infection, and fatigue, but these were mostly mild (57). Of note, 13% of patients experienced ≥1 adverse event, leading to study withdrawal. Importantly, no new or increased incidence of safety issues were identified in this study and the authors concluded that long-term treatment with eltrombopag was generally safe and well tolerated. Overall, our data indicated that eltrombopag may have potential for repurposing for TN-IBC and TNBC in general.

Papaverine, a vasodilator traditionally used to treat vascular spasms, has been reported to primarily target the phosphodiesterase PDE10A and, less potently, other phosphodiesterases, leading to increased intracellular concentrations of cAMP (58). In MDA-MB-231, cell growth has been reported to be inhibited by agents that elevate intracellular cAMP levels, i.e., 8-bromo-cAMP, cholera toxin, forskolin, and papaverine (59,60). Papaverine has also been reported to inhibit mitochondrial complex 1, reducing oxidative phosphorylation and oxygen consumption in cells (61). This latter mechanism has been proposed to explain papaverine's ability to enhance radiation sensitivity of cancer cells, since higher oxygen levels lead to more radiation damage. Papaverine has also been reported to inhibit cell proliferation and migration of non-small cell lung cancer cell lines through allosteric binding directly to CDK5 and inhibiting its activity (62). This drug has also been reported to inhibit a panel of human liver cell lines with IC_{50} values ranging from 1.7 to 52 μM (63). In a different report, papaverine was reported to selectively inhibit the growth of human prostate cancer cell line PC-3 and induce apoptosis (64). Papaverine was identified in a screen for small molecules that sensitize tumor cells to glucose starvation and this effect was confirmed with four different cell lines (65). In a xenograft mouse model using the DLD1 colon cell line, modest *in vivo* anti-tumor activity of papaverine was observed, but a strong combination effect was observed when combined with bevacizumab, an inhibitor of vascular endothelial growth factor (VEGF) (65). In another study, papaverine demonstrated anti-proliferative activity for MCF-7 and MDA-MB-231 breast cancer cell lines (66). Notably, we are the first to report papaverine activity against an IBC cell line and human TNBC cell lines other than MDA-MB-231. In contrast, our data for papaverine showed weak to no activity against MDA-MB-231 (>12 to >20 μM GI_{50}) which may be due to differing culture conditions-we employed spheroid growth instead of traditional 2-D culture. It is well known that spheroid growth can shift the potency of compounds compared to 2-D growth. In follow-up mechanism studies, it will be important to determine if there is a correlation between cAMP elevation or mitochondrial inhibition in papaverine treated cells and cell line sensitivity to this drug. There is an oral form of papaverine available and one study using chronic dosing of oral papaverine reported no adverse events associated with the drug (67). However,

hepatotoxicity in some patients taking oral papaverine has been reported (68).

Mozavaptan is a vasopressin V2 receptor (V2R) antagonist that is primarily used for hyponatremia. In our study, mozavaptan inhibited proliferation of 3 out of 4 TNBC cell lines grown in spheroid form and Hs578T grown in 2-D with a range of GI_{50}s of 2.7-7.6 μM. Mozavaptan has been approved in Japan, but not by the FDA, so we also tested another member of vasopressin receptor antagonist family that is FDA-approved-tolvaptan. Tolvaptan did not show the same activity/potency as mozavaptan. For example, mozavaptan inhibited MDA-MB-231 cells with a GI_{50} of 3.3 μM, but tolvaptan was >20 μM. Tolvaptan has a reported IC_{50} of 0.2 nM for its target in one cell-based assay (69) and mozavaptan has a reported IC_{50} of 19 nM in a CHO V2R expression system (70). Thus, given (1) the high potency of mozavaptan and tolvaptan for V2R in contrast to our relatively high GI_{50} values and (2) inconsistent activity between the two drugs in our study, our data is highly suggestive that the antiproliferative activity of both drugs in our study were due to off-target activity. According to The Human Protein Atlas database (https://www.proteinatlas.org), the RNA level of the V2R gene (AVPR2) was 0.0 normalized transcript per million (nTPM) for MDA-MB-231, SUM-159 and HCC1806, while RNA level for SUM-149 was 1.3 nTPM. Thus, this data indicated a lack of correlation between V2R RNA expression and sensitivity to mozavaptan since we observed mozavaptan activity in the cell lines not expressing V2R RNA, but no activity in SUM-149 that may express some level of V2R RNA (but very low). This database also reports undetectable V2R protein levels in MDA-MB-231 and HCC1806, with no data on the other cell lines. In contrast, one study showed V2R expression in MDA-MB-231 (and MCF-7 and mouse F3II mammary cell line) by immunohistochemistry (71). This same study demonstrated that a synthetic peptide agonist for V2R, desmopressin, was cytostatic in proliferation assays using MDA-MB-231 and reduced tumor growth and angiogenesis in mouse models using MDA-MB-231 and F3II. However, tolvaptan and mozavaptan are both potent antagonists of V2R and thus V2R antagonism as a mechanism would be inconsistent with this prior study. One hypothesis to explain all this data is that V2R does not play a role in the mechanisms for these drugs in our assays and the broad activity observed for mozavaptan is off-target activity for a target not shared by tolvaptan (or same off-target, but differential potency) due to structural differences between the drugs. It was not possible to determine the potency of mozavaptan relative to the C_{max} since this data was not readily available in the literature. Thus, it is difficult to assess the potential for *in vivo* activity of mozavaptan at physiological doses. In terms of adverse events, mozavaptan has been reported to have no serious adverse events, with the most common being dry mouth (72).

Spironolactone is a mineralocorticoid receptor antagonist along with being a nonselective antagonist of androgen and progesterone receptors (73). It functions as a potassium-sparing diuretic that is used to treat high blood pressure, heart failure and other conditions. Spironolactone only had activity against the TN-IBC cell line suggesting some unique target or pathway dependency in this cell line compared to the other TNBC cell lines. Since spironolactone is a weak antagonist of the androgen receptor (AR), it is possible that this was the target in SUM-149. However, it has been reported that SUM-149 does not express AR, but SUM-159 does (74), which does not fit our activity results. Spironolactone has also been reported to be a nucleotide excision repair (NER) inhibitor (75). This mechanism involves spironolactone inducing degradation of the XPB helicase that is part of the TFIIH transcription/repair complex involved in NER. This group also reported no inhibition with 10 μM spironolactone in four- or five-day cell viability assays using HeLa, A2780 and HCT-116 cell lines. These cell lines along with MDA-MB-231, HCC1806 and SUM-159 have wild type BRCA1 (76-80). Unique in our panel, SUM-149 has a BRCA1 frameshift mutation and allele loss that may make it more dependent on remaining DNA repair functions (76). Notably, only 3 out of 41 human breast cancer cell lines had BRCA1 mutations (with allele loss), with SUM-149 being one of them. This DNA repair defect may make SUM-149 more sensitive to inhibition of NER by spironolactone. Thus, the SUM-149-specific sensitivity to spironolactone may be due to a synthetic lethal type response in this cell line and this would explain the unusual sensitivity of SUM-149 to spironolactone. The spironolactone GI_{50} of 3.5 μM against SUM-149 is 10-fold higher than the C_{max} of 0.35 μM. Therefore, it is unclear if it would have any significant activity in humans. Spironolactone has been reported to have no significant impact on the risk of breast cancer in a meta-analysis (81). However, one recent study of younger women taking spironolactone indicated a slight beneficial effect in terms of BC risk (82). If there is a positive impact for the relatively rare IBC, then it would probably not be detectable within a population of mostly non-IBC patients. The common adverse event associated with long-term spironolactone use is menstrual irregularities, which are dose-dependent and can be countered with oral contraceptives or intrauterine devices (83). Other infrequent adverse events include increased urination, lightheadedness, headaches, nausea, vomiting, breast discomfort, and breast enlargement. Since it is a potassium-retaining diuretic, elevated potassium level (hyperkalemia) is another possible side effect, especially in patients with renal dysfunction or heart failure.

The adverse effects of the other identified drugs also provide insight into their potential for re-purposing. For adefovir, the most common adverse events were similar to placebo, except that headache and abdominal pain occurred more frequently with adefovir but did not lead to discontinuation (84). Adefovir is associated with dose-dependent increased risk of renal toxicity and thus, monitoring would be important. For dolutegravir, the most common adverse events reported were diarrhea, fatigue, and headache (85). However, the majority of these adverse events were mild or moderate in severity. Based on a recent analysis of the FDA Adverse Event Reporting System database, dolutegravir treatment decision should also include restrictions on contraindicated populations (e.g. pregnant, hepatobiliary disorders) (86). In a study with healthy volunteers, no serious adverse events occurred during a 7-day study of dronedarone (87). However, dronedarone can induce prolonged RR and QT intervals as a function of dose, without effect on circadian patterns, which suggests potential proarrhythmic risk (88). For the anti-malarial drug halofantrine, clinical studies are short term in nature. The

main serious adverse effect associated with halofantrine use is QT interval prolongation which prevents its use for long term treatment at normal doses (89).

In summary, we identified eltrombopag and papaverine as having anti-proliferative activity against SUM-149 and other TNBC cell lines. Furthermore, these drugs had GI_{50}:C_{max} ratios of 1-2 for sensitive cell lines, suggesting that they are potent enough to potentially have activity *in vivo*. Therefore, these drugs should be further tested against patient-derived organoids (PDO) and xenograft models of TN-IBC and TNBC to assess their activity alone and in combination with other drugs.

Acknowledgements

Not applicable.

Funding

The project described was partially supported by the National Institutes of Health through the RCMI grant NIH/NIMHD (grant no. U54MD012392). This project was also partially funded by internal grants from BRITE at North Carolina Central University.

Availability of data and materials

The data generated in the present study may be requested from the corresponding author. The dataset used in this article to identify candidate non-oncology drugs has been previously published (12) and is publicly available in the PRISM database (https://depmap.org/repurposing).

Authors' contributions

SA performed spheroid-based cell proliferation/cytotoxicity assays, analyzed the results and interpreted the data. SK performed the 2-D cell proliferation/cytotoxicity assays, analyzed the results and interpreted the data. KPW contributed to the conception and design and revision of the manuscript. JES contributed to the conception and design, analysis of the results, interpretation of the data and drafting of the manuscript. SA and SK confirm the authenticity of all the raw data. All authors read and approved the final manuscript.

Ethics approval and consent to participate

Not applicable.

Patient consent for publication

Not applicable.

Competing interests

The authors declare that they have no competing interests.

Authors' information

Kevin P. Williams, ORCID: 0000000269304630; John E. Scott, ORCID: 0000-0002-5987-9334.

References

1. Beňačka R, Szabóová D, Guľašová Z, Hertelyová Z and Radoňák J: Classic and new markers in diagnostics and classification of breast cancer. Cancers (Basel) 14: 5444, 2022.
2. Lee J: Current treatment landscape for early triple-negative breast cancer (TNBC). J Clin Med 12: 1524, 2023.
3. Russnes HG, Lingjærde OC, Børresen-Dale AL and Caldas C: Breast cancer molecular stratification: From intrinsic subtypes to integrative clusters. Am J Pathol 187: 2152-2162, 2017.
4. Devi GR, Hough H, Barrett N, Cristofanilli M, Overmoyer B, Spector N, Ueno NT, Woodward W, Kirkpatrick J, Vincent B, *et al*: Perspectives on inflammatory breast cancer (IBC) research, clinical management and community engagement from the duke IBC consortium. J Cancer 10: 3344-3351, 2019.
5. Boussen H, Berrazaga Y, Sherif K, Manai M, Berrada N, Mejri N, Siala I, Levine PH and Cristofanilli M: Inflammatory breast cancer: Epidemiologic data and therapeutic results. Int Rev Cell Mol Biol 384: 1-23, 2024.
6. Matro JM, Li T, Cristofanilli M, Hughes ME, Ottesen RA, Weeks JC and Wong YN: Inflammatory breast cancer management in the national comprehensive cancer network: The disease, recurrence pattern, and outcome. Clin Breast Cancer 15: 1-7, 2015.
7. Hester RH, Hortobagyi GN and Lim B: Inflammatory breast cancer: Early recognition and diagnosis is critical. Am J Obstet Gynecol 225: 392-396, 2021.
8. Biswas T, Efird JT, Prasad S, James SE, Walker PR and Zagar TM: Inflammatory TNBC breast cancer: Demography and clinical outcome in a large cohort of patients with TNBC. Clin Breast Cancer 16: 212-216, 2016.
9. Chainitikun S, Saleem S, Lim B, Valero V and Ueno NT: Update on systemic treatment for newly diagnosed inflammatory breast cancer. J Adv Res 29: 1-12, 2021.
10. Al Khzem AH, Gomaa MS, Alturki MS, Tawfeeq N, Sarafroz M, Alonaizi SM, Al Faran A, Alrumaihi LA, Alansari FA and Alghamdi AA: Drug repurposing for cancer treatment: A comprehensive review. Int J Mol Sci 25: 12441, 2024.
11. Szalai P and Engedal N: An image-based assay for high-throughput analysis of cell proliferation and cell death of adherent cells. Bio Protoc 8: e2835, 2018.
12. Corsello SM, Nagari RT, Spangler RD, Rossen J, Kocak M, Bryan JG, Humeidi R, Peck D, Wu X, Tang AA, *et al*: Discovering the anti-cancer potential of non-oncology drugs by systematic viability profiling. Nat Cancer 1: 235-248, 2020.
13. Culley J, Nagle PW, Dawson JC and Carragher NO: Patient derived glioma stem cell spheroid reporter assays for live cell high content analysis. SLAS Discov 28: 13-19, 2023.
14. Pfab C, Schnobrich L, Eldnasoury S, Gessner A and El-Najjar N: Repurposing of antimicrobial agents for cancer therapy: What do we know? Cancers (Basel) 13: 3193, 2021.
15. Bhattacharya U, Kamran M, Manai M, Cristofanilli M and Ince TA: Cell-of-origin targeted drug repurposing for triple-negative and inflammatory breast carcinoma with HDAC and HSP90 inhibitors combined with niclosamide. Cancers (Basel) 15: 332, 2023.
16. da Silva Fernandes T, Gillard BM, Dai T, Martin JC, Chaudhry KA, Dugas SM, Fisher AA, Sharma P, Wu R, Attwood KM, *et al*: Inosine monophosphate dehydrogenase 2 (IMPDH2) modulates response to therapy and chemo-resistance in triple negative breast cancer. Sci Rep 15: 1061, 2025.
17. Kim JH, Park S, Jung E, Shin J, Kim YJ, Kim JY, Sessler JL, Seo JH and Kim JS: A dual-action niclosamide-based prodrug that targets cancer stem cells and inhibits TNBC metastasis. Proc Natl Acad Sci USA 120: e2304081120, 2023.
18. Greenshields AL, Fernando W and Hoskin DW: The anti-malarial drug artesunate causes cell cycle arrest and apoptosis of triple-negative MDA-MB-468 and HER2-enriched SK-BR-3 breast cancer cells. Exp Mol Pathol 107: 10-22, 2019.
19. Zadeh T, Lucero M and Kandpal RP: Artesunate-induced cellular effects are mediated by specific EPH receptors and ephrin ligands in breast carcinoma cells. Cancer Genomics Proteomics 19: 19-26, 2022.
20. Liu H, Sun H, Zhang B, Liu S, Deng S, Weng Z, Zuo B, Yang J and He Y: ^{18}F-FDG PET imaging for monitoring the early anti-tumor effect of albendazole on triple-negative breast cancer. Breast Cancer 27: 372-380, 2020.
21. Priotti J, Baglioni MV, Garcia A, Rico MJ, Leonardi D, Lamas MC and Menacho Márquez M: Repositioning of anti-parasitic drugs in cyclodextrin inclusion complexes for treatment of triple-negative breast cancer. AAPS PharmSciTech 19: 3734-3741, 2018.

22. Kieliszek AM, Mobilio D, Bassey-Archibong BI, Johnson JW, Piotrowski ML, de Araujo ED, Sedighi A, Aghaei N, Escudero L, Ang P, *et al*: De novo GTP synthesis is a metabolic vulnerability for the interception of brain metastases. Cell Rep Med 5: 101755, 2024.
23. Benjanuwattra J, Chaiyawat P, Pruksakorn D and Koonrungsesomboon N: Therapeutic potential and molecular mechanisms of mycophenolic acid as an anticancer agent. Eur J Pharmacol 887: 173580, 2020.
24. Abdelwahab MT, Wasserman S, Brust JCM, Gandhi NR, Meintjes G, Everitt D, Diacon A, Dawson R, Wiesner L, Svensson EM, *et al*: Clofazimine pharmacokinetics in patients with TB: Dosing implications. J Antimicrob Chemother 75: 3269-3277, 2020.
25. Bullingham RE, Nicholls AJ and Kamm BR: Clinical pharmacokinetics of mycophenolate mofetil. Clin Pharmacokinet 34: 429-455, 1998.
26. Ceballos L, Alvarez L, Lifschitz A and Lanusse C: Ivermectin systemic availability in adult volunteers treated with different oral pharmaceutical formulations. Biomed Pharmacother 160: 114391, 2023.
27. Friedrich C, Richter E, Trommeshauser D, de Kruif S, van Iersel T, Mandel K and Gessner U: Absence of excretion of the active moiety of bisacodyl and sodium picosulfate into human breast milk: An open-label, parallel-group, multiple-dose study in healthy lactating women. Drug Metab Pharmacokinet 26: 458-464, 2011.
28. Girard PM, Clair B, Certain A, Bidault R, Matheron S, Regnier B and Farinotti R: Comparison of plasma concentrations of aerosolized pentamidine in nonventilated and ventilated patients with pneumocystosis. Am Rev Respir Dis 140: 1607-1610, 1989.
29. Kouakou YI, Tod M, Leboucher G, Lavoignat A, Bonnot G, Bienvenu AL and Picot S: Systematic review of artesunate pharmacokinetics: Implication for treatment of resistant malaria. Int J Infect Dis 89: 30-44, 2019.
30. Milton KA, Edwards G, Ward SA, Orme ML and Breckenridge AM: Pharmacokinetics of halofantrine in man: Effects of food and dose size. Br J Clin Pharmacol 28: 71-77, 1989.
31. Naccarelli GV, Wolbrette DL, Levin V, Samii S, Banchs JE, Penny-Peterson E and Gonzalez MD: Safety and efficacy of dronedarone in the treatment of atrial fibrillation/flutter. Clin Med Insights Cardiol 5: 103-119, 2011.
32. Ross LL, Song IH, Arya N, Choukour M, Zong J, Huang SP, Eley T, Wynne B and Buchanan AM: No clinically significant pharmacokinetic interactions between dolutegravir and daclatasvir in healthy adult subjects. BMC Infect Dis 16: 347, 2016.
33. Schulz M and Schmoldt A: Therapeutic and toxic blood concentrations of more than 800 drugs and other xenobiotics. Pharmazie 58: 447-474, 2003.
34. Schweizer MT, Haugk K, McKiernan JS, Gulati R, Cheng HH, Maes JL, Dumpit RF, Nelson PS, Montgomery B, McCune JS, *et al*: A phase I study of niclosamide in combination with enzalutamide in men with castration-resistant prostate cancer. PLoS One 13: e0198389, 2018.
35. Williams DD, Peng B, Bailey CK, Wire MB, Deng Y, Park JW, Collins DA, Kapsi SG and Jenkins JM: Effects of food and antacids on the pharmacokinetics of eltrombopag in healthy adult subjects: Two single-dose, open-label, randomized-sequence, crossover studies. Clin Ther 31: 764-776, 2009.
36. Xu FG, Zhang ZJ, Dong HJ, Tian Y, Liu Y and Chen Y: Bioequivalence assessment of two formulations of spironolactone in Chinese healthy male volunteers. Arzneimittelforschung 58: 117-121, 2008.
37. Zou J, Di B, Zhang J, Dai L, Ding L, Zhu Y, Fan H and Xiao D: Determination of adefovir by LC-ESI-MS-MS and its application to a pharmacokinetic study in healthy Chinese volunteers. J Chromatogr Sci 47: 889-894, 2009.
38. Abbas ZN, Al-Saffar AZ, Jasim SM and Sulaiman GM: Comparative analysis between 2D and 3D colorectal cancer culture models for insights into cellular morphological and transcriptomic variations. Sci Rep 13: 18380, 2023.
39. Filipiak-Duliban A, Brodaczewska K, Kajdasz A and Kieda C: Spheroid culture differentially affects cancer cell sensitivity to drugs in melanoma and RCC models. Int J Mol Sci 23: 1166, 2022.
40. Li J, Lin J, Lin JR, Farris M, Robbins L, Andrada L, Grohol B, Nong S and Liu Y: Dolutegravir inhibits proliferation and motility of BT-20 tumor cells through inhibition of human endogenous retrovirus type K. Cureus 14: e26525, 2022.
41. Chen M, Hu L, Bao X, Ye K, Li Y, Zhang Z, Kaufmann SH, Xiao J and Dai H: Eltrombopag directly activates BAK and induces apoptosis. Cell Death Dis 14: 394, 2023.
42. Lin Y, Shi Q, Yang G, Shi F, Zhou Y, Wang T, Xu P, Li P, Liu Z, Sun H, *et al*: A small-molecule drug inhibits autophagy gene expression through the central regulator TFEB. Proc Natl Acad Sci USA 120: e2213670120, 2023.
43. Cui C, Pan Y, Zhang C, Zhu D, Xuan Y, Hao P, Ke X, Zhou X and Qu Y: Eltrombopag binds SDC4 directly and enhances MAPK signaling and macropinocytosis in cancer cells. Am J Cancer Res 12: 2697-2710, 2022.
44. Spitz AZ, Zacharioudakis E, Reyna DE, Garner TP and Gavathiotis E: Eltrombopag directly inhibits BAX and prevents cell death. Nat Commun 12: 1134, 2021.
45. Cheraghi S, Senel P, Dogan Topal B, Agar S, Majidian M, Yurtsever M, Bellur Atici E, Gölcü A and Ozkan SA: Elucidation of DNA-eltrombopag binding: electrochemical, spectroscopic and molecular docking techniques. Biosensors (Basel) 13: 300, 2023.
46. Argenziano M, Di Paola A, Tortora C, Di Pinto D, Pota E, Di Martino M, Perrotta S, Rossi F and Punzo F: Effects of iron chelation in osteosarcoma. Curr Cancer Drug Targets 21: 443-455, 2021.
47. Argenziano M, Tortora C, Paola AD, Pota E, Martino MD, Pinto DD, Leva CD and Rossi F: Eltrombopag and its iron chelating properties in pediatric acute myeloid leukemia. Oncotarget 12: 1377-1387, 2021.
48. Waters T, Goss KL, Koppenhafer SL, Terry WW and Gordon DJ: Eltrombopag inhibits the proliferation of Ewing sarcoma cells via iron chelation and impaired DNA replication. BMC Cancer 20: 1171, 2020.
49. Dogra N, Singh P and Kumar A: A multistep in silico approach identifies potential glioblastoma drug candidates via inclusive molecular targeting of glioblastoma stem cells. Mol Neurobiol 61: 9253-9271, 2024.
50. Erickson-Miller CL, Pillarisetti K, Kirchner J, Figueroa DJ, Ottesen L, Martin AM, Liu Y, Kamel YM and Messam C: Low or undetectable TPO receptor expression in malignant tissue and cell lines derived from breast, lung, and ovarian tumors. BMC Cancer 12: 405, 2012.
51. Idlin N, Krishnamoorthy S, Wolczyk M, Fakhri M, Lechowski M, Stec N, Milek J, Mandal PK, Cendrowski J, Spanos C, *et al*: Effects of genetic ablation and pharmacological inhibition of HuR on gene expression, iron metabolism, and hormone levels. BMC Biol 23: 24, 2025.
52. Roth M, Will B, Simkin G, Narayanagari S, Barreyro L, Bartholdy B, Tamari R, Mitsiades CS, Verma A and Steidl U: Eltrombopag inhibits the proliferation of leukemia cells via reduction of intracellular iron and induction of differentiation. Blood 120: 386-394, 2012.
53. Zhu Y, Yang L, Xu J, Yang X, Luan P, Cui Q, Zhang P, Wang F, Li R, Ding X, *et al*: Discovery of the anti-angiogenesis effect of eltrombopag in breast cancer through targeting of HuR protein. Acta Pharm Sin B 10: 1414-1425, 2020.
54. Chen Y, Zhang R, Yang L, Zhang P, Wang F, Lin G, Zhang J and Zhu Y: Eltrombopag inhibits metastasis in breast carcinoma by targeting HuR protein. Int J Mol Sci 24: 3164, 2023.
55. Jenkins JM, Williams D, Deng Y, Uhl J, Kitchen V, Collins D and Erickson-Miller CL: Phase 1 clinical study of eltrombopag, an oral, nonpeptide thrombopoietin receptor agonist. Blood 109: 4739-4741, 2007.
56. Shen CL, Hsieh TC, Wang TF, Huang WH, Chu SC and Wu YF: Designing a scoring system for differential diagnosis from reactive thrombocytosis and essential thrombocytosis. Front Med (Lausanne) 8: 736150, 2021.
57. Saleh MN, Bussel JB, Cheng G, Meyer O, Bailey CK, Arning M and Brainsky A; EXTEND Study Group: Safety and efficacy of eltrombopag for treatment of chronic immune thrombocytopenia: Results of the long-term, open-label EXTEND study. Blood 121: 537-545, 2013.
58. Bhat A, Tan V, Heng B, Chow S, Basappa S, Essa MM, Chidambaram SB and Guillemin GJ: Papaverine, a phosphodiesterase 10A inhibitor, ameliorates quinolinic acid-induced synaptotoxicity in human cortical neurons. Neurotox Res 39: 1238-1250, 2021.
59. Fontana JA, Miksis G, Miranda DM and Durham JP: Inhibition of human mammary carcinoma cell proliferation by retinoids and intracellular cAMP-elevating compounds. J Natl Cancer Inst 78: 1107-1112, 1987.
60. Gomes DA, Joubert AM and Visagie MH: In vitro effects of papaverine on cell proliferation, reactive oxygen species, and cell cycle progression in cancer cells. Molecules 26: 6388, 2021.
61. Benej M, Hong X, Vibhute S, Scott S, Wu J, Graves E, Le QT, Koong AC, Giaccia AJ, Yu B, *et al*: Papaverine and its derivatives radiosensitize solid tumors by inhibiting mitochondrial metabolism. Proc Natl Acad Sci USA 115: 10756-10761, 2018.

62. Laure A, Royet C, Bihel F, Baratte B, Bach S, Peyressatre M and Morris MC: Ethaverine and papaverine target cyclin-dependent kinase 5 and inhibit lung cancer cell proliferation and migration. ACS Pharmacol Transl Sci 7: 1377-1385, 2024.
63. Sahin ID, Christodoulou MS, Guzelcan EA, Koyas A, Karaca C, Passarella D and Cetin-Atalay R: A small library of chalcones induce liver cancer cell death through Akt phosphorylation inhibition. Sci Rep 10: 11814, 2020.
64. Huang H, Li LJ, Zhang HB and Wei AY: Papaverine selectively inhibits human prostate cancer cell (PC-3) growth by inducing mitochondrial mediated apoptosis, cell cycle arrest and down-regulation of NF-κB/PI3K/Akt signalling pathway. J BUON 22: 112-118, 2017.
65. Marciano R, Prasad M, Ievy T, Tzadok S, Leprivier G, Elkabets M and Rotblat B: High-throughput screening identified compounds sensitizing tumor cells to glucose starvation in culture and VEGF inhibitors in vivo. Cancers (Basel) 11: 156, 2019.
66. Sajadian S, Vatankhah M, Majdzadeh M, Kouhsari SM, Ghahremani MH and Ostad SN: Cell cycle arrest and apoptogenic properties of opium alkaloids noscapine and papaverine on breast cancer stem cells. Toxicol Mech Methods 25: 388-395, 2015.
67. Gardos G, Cole JO and Sniffin C: An evaluation of papaverine in tardive dyskinesia. J Clin Pharmacol 16: 304-310, 1976.
68. Shupack J, Stiller M, Meola T Jr and Orbuch P: Papaverine hydrochloride in the treatment of atopic dermatitis: A double-blind, placebo-controlled crossover clinical trial to reassess safety and efficacy. Dermatologica 183: 21-24, 1991.
69. Reif GA, Yamaguchi T, Nivens E, Fujiki H, Pinto CS and Wallace DP: Tolvaptan inhibits ERK-dependent cell proliferation, Cl^- secretion, and in vitro cyst growth of human ADPKD cells stimulated by vasopressin. Am J Physiol Renal Physiol 301: F1005-F1013, 2011.
70. Tahara A, Saito M, Sugimoto T, Tomura Y, Wada K, Kusayama T, Tsukada J, Ishii N, Yatsu T, Uchida W and Tanaka A: Pharmacological characterization of the human vasopressin receptor subtypes stably expressed in Chinese hamster ovary cells. Br J Pharmacol 125: 1463-1470, 1998.
71. Garona J, Pifano M, Orlando UD, Pastrian MB, Iannucci NB, Ortega HH, Podesta EJ, Gomez DE, Ripoll GV and Alonso DF: The novel desmopressin analogue [V4Q5]dDAVP inhibits angiogenesis, tumour growth and metastases in vasopressin type 2 receptor-expressing breast cancer models. Int J Oncol 46: 2335-2345, 2015.
72. Ectopic ADH Syndrome Therapeutic Research Group; Yamaguchi K, Shijubo N, Kodama T, Mori K, Sugiura T, Kuriyama T, Kawahara M, Shinkai T, Iguchi H and Sakurai M: Clinical implication of the antidiuretic hormone (ADH) receptor antagonist mozavaptan hydrochloride in patients with ectopic ADH syndrome. Jpn J Clin Oncol 41: 148-152, 2011.
73. Ferreira JP, Pitt B and Zannad F: Mineralocorticoid receptor antagonists in heart failure: An update. Circ Heart Fail 17: e011629, 2024.
74. Ethier SP, Guest ST, Garrett-Mayer E, Armeson K, Wilson RC, Duchinski K, Couch D, Gray JW and Kappler C: Development and implementation of the SUM breast cancer cell line functional genomics knowledge base. NPJ Breast Cancer 6: 30, 2020.
75. Alekseev S, Ayadi M, Brino L, Egly JM, Larsen AK and Coin F: A small molecule screen identifies an inhibitor of DNA repair inducing the degradation of TFIIH and the chemosensitization of tumor cells to platinum. Chem Biol 21: 398-407, 2014.
76. Elstrodt F, Hollestelle A, Nagel JHA, Gorin M, Wasielewski M, van den Ouweland A, Merajver SD, Ethier SP and Schutte M: BRCA1 mutation analysis of 41 human breast cancer cell lines reveals three new deleterious mutants. Cancer Res 66: 41-45, 2006.
77. Martín-Bejarano P, Sánchez-Tapia EM, Jessica P, Martín-Gómez T, Tocino RV, González-Sarmiento R and Herrero AB: Functional characterization of BRCA1 variants of unknown significance using homologous recombination repair assays. Breast Cancer Res 27: 174, 2025.
78. Baloch T, López-Ozuna VM, Wang Q, Matanis E, Kessous R, Kogan L, Yasmeen A and Gotlieb WH: Sequential therapeutic targeting of ovarian cancer harboring dysfunctional BRCA1. BMC Cancer 19: 44, 2019.
79. Mita P, Sun X, Fenyö D, Kahler DJ, Li D, Agmon N, Wudzinska A, Keegan S, Bader JS, Yun C and Boeke JD: BRCA1 and S phase DNA repair pathways restrict LINE-1 retrotransposition in human cells. Nat Struct Mol Biol 27: 179-191, 2020.
80. Keung MY, Wu Y, Badar F and Vadgama JV: Response of breast cancer cells to PARP inhibitors is independent of BRCA status. J Clin Med 9: 940, 2020.
81. Bommareddy K, Hamade H, Lopez-Olivo MA, Wehner M, Tosh T and Barbieri JS: Association of spironolactone use with risk of cancer: A systematic review and meta-analysis. JAMA Dermatol 158: 275-282, 2022.
82. Garate D, Thang CJ, Golovko G, Wilkerson MG and Barbieri JS: A matched cohort study evaluating whether spironolactone or tetracycline-class antibiotic use among female acne patients is associated with breast cancer development risk. Arch Dermatol Res 316: 196, 2024.
83. Lin G, Chen R, Wen C, Li Z, Yan X and Li L: Analyzing real-world adverse events of spironolactone with the FAERS database. PLoS One 20: e0330659, 2025.
84. Kayaaslan B and Guner R: Adverse effects of oral antiviral therapy in chronic hepatitis B. World J Hepatol 9: 227-241, 2017.
85. Min S, Sloan L, DeJesus E, Hawkins T, McCurdy L, Song I, Stroder R, Chen S, Underwood M, Fujiwara T, *et al*: Antiviral activity, safety, and pharmacokinetics/pharmacodynamics of dolutegravir as 10-day monotherapy in HIV-1-infected adults. AIDS 25: 1737-1745, 2011.
86. Su J, He L and Wang M: Post-marketing safety concerns with dolutegravir: A pharmacovigilance study based on the FDA adverse event reporting system database. Front Pharmacol 16: 1625601, 2025.
87. Tschuppert Y, Buclin T, Rothuizen LE, Decosterd LA, Galleyrand J, Gaud C and Biollaz J: Effect of dronedarone on renal function in healthy subjects. Br J Clin Pharmacol 64: 785-791, 2007.
88. Wadhani N, Sarma JS, Singh BN, Radzik D and Gaud C: Dose-dependent effects of oral dronedarone on the circadian variation of RR and QT intervals in healthy subjects: Implications for antiarrhythmic actions. J Cardiovasc Pharmacol Ther 11: 184-190, 2006.
89. Charbit B, Becquemont L, Lepère B, Peytavin G and Funck-Brentano C: Pharmacokinetic and pharmacodynamic interaction between grapefruit juice and halofantrine. Clin Pharmacol Ther 72: 514-523, 2002.